ORNL/TM-2014/556

Corrosion Assessment of Candidate Materials for the SHINE Subcritical Assembly Vessel and Components—2014 Report

S. J. Pawel

October 2014

Approved for public release;
distribution is unlimited.

OAK RIDGE NATIONAL LABORATORY
MANAGED BY UT-BATTELLE FOR THE US DEPARTMENT OF ENERGY

DOCUMENT AVAILABILITY

Reports produced after January 1, 1996, are generally available free via US Department of Energy (DOE) SciTech Connect.

Website http://www.osti.gov/scitech/

Reports produced before January 1, 1996, may be purchased by members of the public from the following source:

National Technical Information Service
5285 Port Royal Road
Springfield, VA 22161
Telephone 703-605-6000 (1-800-553-6847)
TDD 703-487-4639
Fax 703-605-6900
E-mail info@ntis.gov
Website http://www.ntis.gov/help/ordermethods.aspx

Reports are available to DOE employees, DOE contractors, Energy Technology Data Exchange representatives, and International Nuclear Information System representatives from the following source:

Office of Scientific and Technical Information
PO Box 62
Oak Ridge, TN 37831
Telephone 865-576-8401
Fax 865-576-5728
E-mail reports@osti.gov
Website http://www.osti.gov/contact.html

This report was prepared as an account of work sponsored by an agency of the United States Government. Neither the United States Government nor any agency thereof, nor any of their employees, makes any warranty, express or implied, or assumes any legal liability or responsibility for the accuracy, completeness, or usefulness of any information, apparatus, product, or process disclosed, or represents that its use would not infringe privately owned rights. Reference herein to any specific commercial product, process, or service by trade name, trademark, manufacturer, or otherwise, does not necessarily constitute or imply its endorsement, recommendation, or favoring by the United States Government or any agency thereof. The views and opinions of authors expressed herein do not necessarily state or reflect those of the United States Government or any agency thereof.

ORNL/TM-2014/556

Materials Science and Technology Division

CORROSION ASSESSMENT OF CANDIDATE MATERIALS FOR THE SHINE SUBCRITICAL ASSEMBLY VESSEL AND COMPONENTS—FY 2014 REPORT

S. J. Pawel

Date Published: October 2014

Prepared by
OAK RIDGE NATIONAL LABORATORY
Oak Ridge, Tennessee 37831-6283
managed by
UT-BATTELLE, LLC
for the
US DEPARTMENT OF ENERGY
under contract DE-AC05-00OR22725

CONTENTS

Page

LIST OF FIGURES v
LIST OF TABLES vii
ACKNOWLEDGMENTS ix
ABSTRACT xi
1. INTRODUCTION 1
2. LITERATURE REVIEW 1
3. EXPERIMENTAL PROCEDURE 8
3.1 LABORATORY TESTING WITH DEPLETED URANIUM 8
3.1.1 Corrosion test environments 8
3.1.2 Corrosion test materials 10
3.1.3 Corrosion test methods 12
4. RESULTS AND DISCUSSION 17
5. CONCLUSIONS 33
6. REFERENCES 34

LIST OF FIGURES

Figures **Page**

Fig. 1. Corrosion rates of stainless alloys at 20˚C as a function of sulfuric acid concentration in unaerated water. 7
Fig. 2. Corrosion rate of austenitic stainless steels as a function of temperature in 3% sulfuric acid (in water). 8
Fig. 3. Photograph of water bath during testing (upper left) and schematic drawings of flask placement within the water bath and specimen placement within a flask. 12
Fig. 4. Schematic diagram of the planned-interval test strategy. 13
Fig. 5. Schematic diagram of an assembly with three pairs of potential galvanic couples (left) and an actual assembly (right). 14
Fig. 6. Key components of a vibratory horn (left) and details of a cavitation test specimen (right). 15
Fig. 7. Schematic diagram of the cavitation test container and relationship to horn/specimen. 16
Fig. 8. Schematic diagram of an irradiation test vessel (left) along with an actual container lid with various attachments shown. 17
Fig. 9. Range of discoloration observed on Zr-4 specimens as a function of the indicated exposure conditions. 18
Fig. 10. Surface of 304L and 17-4 PH specimens following exposure at 94˚C in uranyl sulfate at a concentration corresponding to 140 g dU/L and 0.25 M excess sulfuric acid. 19
Fig. 11. Average ambient pH values as a function of uranyl sulfate and excess acid concentration for the static exposure results in Tables 7-9. 21
Fig. 12. Surface of primary candidate specimens following exposure at 94˚C in uranyl sulfate at a concentration corresponding to 140 g dU/L with 1 M excess sulfuric acid and 0.25 M excess nitric acid additions for about 96 h. 23
Fig. 13. Surface of 304L and 17-4 PH specimens following exposure at 94˚C in depleted uranyl sulfate at a concentration corresponding to 140 g dU/L with 1 M excess sulfuric acid and 0.25 M excess nitric acid additions for about 96 h. 23
Fig. 14. Type 2304 stainless steel coupons following planned-interval testing for eight total days in a solution containing 140 g dU/L with 0.10 M sulfuric acid and 28 wppm iodine species at 94˚C. 27
Fig. 15. Type 17-4 PH stainless steel planned-interval test coupons following exposure immersed in 140 g dU/L with 0.10 M excess sulfuric acid, 28 wppm iodine species, and 0.25 M nitric acid at 93-94˚C. 29
Fig. 16. Representative appearance of specimens following galvanic exposure in the given conditions. 31
Fig. 17. Weight loss as a function of sonication time for Zr-4 (top) and 17-4 PH (bottom). 32

LIST OF TABLES

Tables **Page**

Table 1. Corrosion rates observed for various materials in flow loop experiments for the HRT design. 2
Table 2. Composition (wt %) boundaries for primary constituents of commonly used stainless steel alloys. 3
Table 3. Corrosion rates of type 347 stainless steel in static uranyl sulfate solutions as a function of temperature. 4
Table 4. Corrosion rates for Zr and Zr-2 as a function of temperature in static exposures in oxygenated 0.04 M UO_2SO_4 + 0.02 M H_2SO_4 + 0.005 M $CuSO_4$ without the presence of ionizing radiation 6
Table 5. Composition (wt %) for stainless steel alloys. 11
Table 6. Composition (wt %) for zirconium-based alloys. 11
Table 7. Corrosion rates calculated from weight change for specimens exposed in uranyl sulfate corresponding to a concentration of 140 g dU/L, as a function of excess acid addition and temperature. 18
Table 8. Corrosion rates calculated from weight change for specimens exposed in uranyl sulfate corresponding to a concentration of 70 g dU/L as a function of excess acid addition and temperature. 20
Table 9. Corrosion rates calculated from weight change for specimens exposed in uranyl sulfate corresponding to a concentration of 280 g dU/L as a function of excess acid addition and temperature. 20
Table 10. Corrosion rates calculated from weight change for specimens exposed in uranyl sulfate corresponding to concentrations of 140 and 280 g dU/L with 0.25 M added nitric acid as a function of excess sulfuric acid addition at 80°C. 21
Table 11. Corrosion rates calculated from weight change for specimens exposed in uranyl sulfate corresponding to a concentration of 140 g dU/L with 1 M added sulfuric acid as a function of excess nitric acid addition at 93–94°C. 22
Table 12. Corrosion rates calculated from weight change for specimens exposed in uranyl sulfate corresponding to a concentration of 70 or 140 g dU/L with 50 wppm iodine species added as a function of excess sulfuric acid addition at 93–94°C. 24
Table 13. Planned-interval test results for stainless steels exposed (immersion and vapor) to test solutions with 140 g dU/L and 0.10 M excess sulfuric acid as a function of iodine species additions at 93–94°C 26
Table 14. Stainless steel corrosion rates as a function of iodine concentration for solutions of 140 g dU/L and 0.10 M excess sulfuric acid at 93–94°C 26
Table 15. Planned-interval test results for stainless steels exposed (immersion and vapor) to test solutions of 140 g dU/L and 0.10 M excess sulfuric acid with 28 wppm iodine species, with and without 0.25 M nitric acid addition, at 93–94°C 28
Table 16. Summary of galvanic couple exposure test combinations 30

ACKNOWLEDGMENTS

This research project was sponsored by the US Department of Energy National Nuclear Security Administration under the Global Threat Reduction Initiative to support promising technologies for the production of ^{99}Mo. The program is managed at Oak Ridge National Laboratory by C. D. Bryan and supported by a number of other individuals owed thanks by the author. In particular, Z. M. Burns performed a number of laboratory corrosion tests and managed laboratory supplies as well as specimen procurement, preparation, and cleaning; and H. M. Meyer III performed the x-ray photoelectron spectroscopy studies. N. D. Foster and C. A. Maples provided support associated with procurement and inventory of radioactive materials and associated handling protocol; and K. E. King, B. D. Johnson, and K. P. Curtis performed regular health physics monitoring of the laboratory area as well as various specimens and materials. T. W. Strader and the Health, Safety, and Environment Group provided general support and oversight of the laboratory activities. P. A. Taylor claimed lightly "used" uranyl sulfate solutions as feedstock for another experiment. K. J. Leonard provided zirconium-based materials for specimen making and led the design effort associated with the gamma-irradiation exposure campaign. J. K. Thomson, D. F. Wilson, and B. A. Pint reviewed the manuscript and offered helpful suggestions, and technical editing and final formatting and document handling was supported by D. M. Counce.

E. N. Van Abel and J. Driscoll of SHINE Medical Technologies participated in directing of the laboratory efforts as well as review of the report manuscript.

ABSTRACT

Laboratory corrosion testing of candidate alloys—including Zr-4 and Zr-2.5Nb representing the target solution vessel, and 316L, 2304, 304L, and 17-4 PH stainless steels representing process piping and balance-of-plant components—was performed in support of the proposed SHINE process to produce ^{99}Mo from low-enriched uranium. The test solutions used depleted uranyl sulfate in various concentrations and incorporated a range of temperatures, excess sulfuric acid concentrations, nitric acid additions (to simulate radiolysis product generation), and iodine additions. Testing involved static immersion of coupons in solution and in the vapor above the solution, and was extended to include planned-interval tests to examine details associated with stainless steel corrosion in environments containing iodine species. A large number of galvanic tests featuring couples between a stainless steel and a zirconium-based alloy were performed, and limited vibratory horn testing was incorporated to explore potential erosion/corrosion features of compatibility.

In all cases, corrosion of the zirconium alloys was observed to be minimal, with corrosion rates based on weight loss calculated to be less than 0.1 mil/year with no change in surface roughness. The resulting passive film appeared to be ZrO_2 with variations in thickness that influence apparent coloration (toward light brown for thicker films). Galvanic coupling with various stainless steels in selected exposures had no discernable effect on appearance, surface roughness, or corrosion rate. Erosion/corrosion behavior was the same for zirconium alloys in uranyl sulfate solutions and in sodium sulfate solutions adjusted to a similar pH, suggesting there was no negative effect of uranium resulting from fluid dynamic conditions aggressive to the passive film.

Corrosion of the candidate stainless steels was similarly modest across the entire range of exposures. However, some sensitivity to corrosion of the stainless steels was observed in solutions with 50 wppm iodine (the actual SHINE process expects 0.1–1 wppm) with the highest corrosion rates (up to ~6 mil/year) observed on specimens exposed in the vapor phase. Lower concentrations of iodine species (5 or 28 wppm) proved much less corrosive, and the planned-interval data indicated that metal corrodibility decreased with time for all immersed exposures and, with one minor exception, all vapor exposures. Little change in susceptibility to corrosion was observed as a result of nitric acid additions to the test environment (simulating radiolysis products). The trend toward reduced corrosion (immersion and vapor phase) with decreasing iodine concentration suggests that, at the expected conditions in the SHINE process, it is unlikely that iodine species will generate a general corrosion concern for the candidate stainless steels.

1. INTRODUCTION

Molybdenum-99 (^{99}Mo) is commercially valuable chiefly because it is the parent isotope to the meta-stable gamma-emitting daughter radioisotope technicium-99m (^{99m}Tc). Technicium-99m is commonly used in nuclear imaging associated with cancer detection and in diagnostic tests of the functioning of internal organs such as the kidneys, heart, and brain. Historically, ^{99}Mo has been produced as a fission product in research reactors—at a very limited number of locations around the world—using highly enriched uranium (HEU). At issue, however, is that these reactors are operating well past their design lives and have recently experienced unplanned shutdowns [1,2] that seriously disrupted ^{99}Mo availability and led to substantial price increases. Further, the primary supplier of ^{99}Mo in the western hemisphere—the National Research Universal reactor in Chalk River, Canada—is scheduled to cease production of ^{99}Mo soon (~2016) and is presently licensed to operate only until 2021. Thus, with demand increasing each year, a replacement source of ^{99}Mo is required to avoid delays or cancellations of medical procedures.

The Department of Energy's National Nuclear Security Administration is promoting efforts to establish a reliable domestic supply of ^{99}Mo while eliminating the use of HEU under its Global Threat Reduction Initiative to guard against nuclear proliferation. In response, an alternative ^{99}Mo production method is being developed by SHINE* Medical Technologies in partnership with Phoenix Nuclear Labs. In the new method, a deuteron ion beam is accelerated into a target chamber containing tritium. The resulting interactions produce a high yield of neutrons, which then enter a multiplier layer that increases the neutron population by a factor of about three. After multiplication, the neutrons enter an aqueous target solution containing low-enriched uranium (LEU) in the form of acidified uranyl sulfate. In the target solution, ^{99}Mo and other important radionuclides, such as ^{133}Xe and ^{131}I, are formed by sub-critical fissioning of ^{235}U. After irradiation, the isotopes (^{99}Mo and others of interest) are isolated in a chemical separation process. Compared with current technology, this new technique offers two major advantages: LEU rather than HEU is the fissionable material (this removes the threat of nuclear proliferation and complies with US and international efforts to eliminate civilian use of HEU); and it uses an accelerator which, compared with a reactor scheme, enjoys a reputation for safer, more stable operation for generating neutrons.

Although many aspects of the process have been demonstrated to the satisfaction of various investors as well as the Department of Energy, regulatory authorities such as the Nuclear Regulatory Commission are interested in assurances related to health and safety for workers and the environment before approvals are granted to construct and operate a full-scale facility. To support the necessary assessments, Oak Ridge National Laboratory (ORNL) was tasked with examination of the corrosion properties of candidate materials to be used in the target solution vessel (zirconium alloys) and balance-of-plant support piping (various stainless steels) in solutions representative of the SHINE process in the *absence* of process irradiation. Ultimately, more limited testing of materials under gamma irradiation conditions (radiolysis) is also planned to examine the sensitivity of corrosion to this factor.

2. LITERATURE REVIEW

There is very little relevant information in the open literature regarding the corrosion resistance of zirconium alloys and stainless steels in aqueous uranyl sulfate at the modestly elevated (60–80°C) temperature expected in the SHINE process. Perhaps the most useful information can be found within reports related to execution of the Homogenous Reactor Test (HRT) and related Homogenous Reactor Experiments (HRE) -1 and -2 in the 1950s at ORNL. Although much of this work probably was

* The name SHINE is an acronym for Subcritical Hybrid Intense Neutron Emitter.

documented in a variety of ORNL and other participating laboratory technical memorandums/reports—some available and others unavailable owing to the ravages of time and limited computerized searching of material from that period—many of the key aspects were captured in a textbook-style compendium entitled *Fluid Fuel Reactors* [3] published in 1958. Part I of that summary was dedicated to aqueous homogenous reactors, a review of more than 10 years of research and development at ORNL and other supporting organizations. Of particular relevance to the present task, Chapter 5 of Part I summarizes materials compatibility testing. Supported by information located in other reports [4,5], the following discussion summarizes corrosion data of interest to the SHINE process testing.

Table 1 summarizes corrosion rates observed in experiments conducted in support of the HRT design. The data result from a closed-loop experiment in 0.17 M UO_2SO_4 at 250°C with a flow rate maintained in the range of 3–5 m/s and pressurized with oxygen. (The expected gU/L in the SHINE process is about 3.5 times this concentration.) No ionizing radiation field, as might be expected in an actual homogenous reactor operation, was included. The exposure duration for most experiments was 200 h, but some tests were terminated after shorter times to examine initial corrosion rates. The austenitic stainless steels examined, which included a number of relatively common alloys of similar (but not identical) composition, were observed to corrode at rates in the range of 14–65 mil/year (1 mil = 0.001 in. ≈ 25 µm). The authors pointed out that the corrosion rates given for the stainless alloys represented those observed for short-term exposures (< 100 h exposure), whereas those observed for extended exposures dropped to the order of 0.1–1.0 mil/year after the passive film was more fully formed/stable. No tendency toward intergranular attack in the stainless alloys, even for sensitized material, was observed in the weight loss data or post-test metallography. Static exposures of up to 2000 h in duration in similar solutions at 100 and at 250°C were also performed and confirmed very low corrosion rates (on the order of 0.1 mil/year).

Table 1. Corrosion rates observed for various materials in flow loop experiments for the HRT design. Test conditions include 0.17 M UO_2SO_4 at 250°C and 3–5 m/s flow rate for up to 200 h; closed loop pressurized with 200 psig oxygen

Material class	Rate (mil/year)
Austenitic stainless steels (304, 304L, 316, 316L, 321, 347)	14–65
Zirconium-based alloys (pure Zr, Zr-2)	< 0.01
Nickel-based alloys (Hastelloys C,X; Inconel 600, alloy 25)	120–340
Gold, platinum	< 0.01
Quartz	58
Pyrex glass	730

Data adapted from J. A. Lane, H. G. McPherson, and Frank Maslan, eds., *Fluid Fuel Reactors*, Addison-Wesley, 1958 [3].

In the same tests, the zirconium-based alloys were found to be essentially immune to corrosion and not to undergo detectable weight changes. Expanded testing of the zirconium alloys indicated that this was true of zirconium-based alloys over a wide range of uranyl sulfate concentrations, temperatures, and flow rates in the flow loop experiments, and in static tests at a similar range of temperatures and sulfate concentrations up to 2000 h in duration. It is interesting that gold and platinum were also found to be essentially immune to corrosion in these laboratory test conditions. It appears that gold and platinum were included in early testing in support of HRT primarily because it was thought—at least early in the design stage—that these metals might be the only ones resistant to some of the early solutions under consideration, such as highly concentrated phosphoric acid and highly concentrated uranyl nitrate and

sulfate solutions. As a result, gold and platinum were being considered as plating materials for stainless steels and perhaps other alloys.

The nickel-based alloys appeared to be quite susceptible to corrosion in the test results captured in Table 1; but the authors of *Fluid Fuel Reactors* [3], from which Table 1 was adapted, noted that the corrosion rates dropped to the order of ~ 0.5 mil/year if the test temperature was reduced to 100°C or less as measured in static tests up to 2000 h in duration. Similar corrosion rates were observed for some cobalt-based alloys that were also tested (but not included in Table 1).

Data for quartz (100% SiO_2) and Pyrex (borosilicate material at ~81% SiO_2, 13% B_2O_3, 4% Na_2O, and 2% Al_2O_3) are included to indicate the potential sensitivity to glass composition in these kinds of solutions, should requirements for sight glass, glass columns, or glass-lined components arise. Related to the potential use of glass, the authors of *Fluid Fuel Reactors* [3] also pointed out that the presence of silicates (as deposit surfaces or dissolved in solution) tended to cause/encourage precipitation of uranium from the solution. Among the mineral materials examined, sapphire (at 17 mil/year) was the most resistant.

Most of the stainless steel exposure data gathered in support of the HRT and related reactor operations (HRE-1 and HRE-2) were for type 347 stainless steel. At that time, this grade of stainless steel was very commonly used, whereas today, types 304L or 316L are much more common for the same kinds of service. Type 347 stainless steel is very similar to type 304 in generic composition (see Table 2), with the primary difference being that the former is alloyed with niobium in an attempt to limit weld-related corrosion issues. Ideally, the niobium would form niobium carbides preferentially (over chromium carbides) to improve the intergranular corrosion resistance of the alloy in a variety of environments. This alloying strategy, termed "stabilization," was intended to improve corrosion resistance for alloys exposed to temperatures in the range of 500–700°C arising as a result of service temperatures, stress relief treatments, weld repair thermal cycles, or other similar requirements. Those conditions sometimes presented corrosion problems for the roughly equivalent alloy (304) that was not alloyed with niobium. In the intervening years, decarburization practices at foundries improved substantially, and many carbide-related corrosion problems were eliminated simply by lowering the carbon content substantially (to generate alloys designated 304L and 316L, the low-carbon versions of 304 and 316). Based on the similarity in composition, all three alloys are expected to have comparable corrosion resistance to solutions expected in the SHINE process, but some subtle differences will be explored in a subsequent paragraph of this discussion.

Table 2. Composition (wt %) boundaries for primary constituents of commonly used stainless steel alloys. For comparison, note that the primary difference between the 304 and 316 compositions shown and the "L" grade equivalents is that the carbon content of the latter is limited to a maximum of 0.03%

Element	304	304L	347	316	316L	317L
Cr	18–20	18–20	17–19	16–18	16–18	18–20
Mn	2	2	2	2	2	2
Mo	–	–	–	2–3	2–3	3–4
Si	1	1	1	1	1	1
C	<0.08	<0.03	<0.08	<0.08	<0.03	<0.03
Nb	–		×10%C	–	–	–

An example of the type 347 corrosion data collected appears in Table 3. The experimental results were intended to show the effects of solution temperature and composition, in static autoclaves, on the corrosion rate of type 347 stainless steel in the absence of ionizing radiation. The exposure time was not

explicitly reported but was implied to be ~100 h. The amount of dissolved oxygen in each test solution was not reported, but the authors commented that all tests included 50–1000 ppm oxygen in an effort to prevent reduction and precipitation of uranium in solution. When uranium precipitation was allowed to occur, additional sulfuric acid tended to form in solution, thus increasing the corrosivity toward stainless steels. Although it was not explicitly explained, it seems that the source of the very high oxygen levels was an overpressure of oxygen within the autoclaves for many of the tests. Oxygen overpressures of this type, and oxygen control in general, are not presently planned for the SHINE process; however, literature data and test results are reported herein regarding the use of a slight excess of sulfuric acid to retain uranium in solution.

Table 3. Corrosion rates of type 347 stainless steel in static uranyl sulfate solutions as a function of temperature. All solutions contained 50–1000 ppm oxygen to prevent reduction and precipitation of uranium

Solute concentration (M)			Test temp (°C)	Corrosion rate (mil/year)
UO_2SO_4	H_2SO_4	$CuSO_4$		
0.02	0.006		100	0.25
0.02	0.006		150	0.96
0.04	0.006	0.005	150	0.87
0.04	0.006	0.005	175	5.4
1.3			100	0.40
1.3			125	0.80
1.3			150	2.8
1.3			175	18.0

Data adapted from J. A. Lane, H. G. McPherson, and Frank Maslan, eds, *Fluid Fuel Reactors*, Addison-Wesley, 1958 [3].

The data in Table 3 indicate that corrosion of type 347 steel was perhaps sensitive to temperatures above about 100–125°C, but below that temperature range, corrosion was quite minimal. In contrast, the corrosion rate did seem sensitive to solute concentration (mainly uranyl sulfate) for these test conditions. The authors noted that for temperatures < 100°C, corrosion rates were trivial, and the metallic luster on type 347 steel was retained for very long times before the formation of a thin tarnish film. At higher exposure temperatures, a darker/thicker film formed, but no preferential leaching from the substrate was observed. For exposure temperatures below 175°C, x-ray diffraction studies of the passive film on type 347 steel indicated mixed ferric and chromic oxides that were partially hydrated. Higher exposure temperatures led to the same oxide mix, except that it had become anhydrous.

Other experiences with type 347 stainless steel, in actual reactor experiments as well as lab testing (without ionizing radiation incorporated), included the following observations [3].

- Type 347 stainless steel was used as a major material of construction for the processing portion of both HRE-1 and HRE-2 operating with uranyl sulfate solutions as the fuel, and no failures related to material corrosion were identified.

- Coupling to more noble metals, for example, gold or platinum, did not accelerate corrosion of type 347 stainless steel in uranyl sulfate solutions.

- Even in the unstabilized and/or sensitized condition (formation of carbides on grain boundaries), no intergranular corrosion or accelerated attack of type 347 stainless steel in uranyl sulfate solutions was observed in static autoclave tests.

- Localized crevice and/or pitting attack was not observed in any exposure; it was speculated that maintaining at least 500 ppm oxygen in solution essentially guaranteed the absence of localized attack.

- Stress-corrosion cracking of type 347 steel was observed only in the presence of dissolved chlorides (>5 ppm) at elevated temperatures (>100°C). (Both of these apparent thresholds exceed the exposure boundaries expected for the SHINE process.) Other halides were expected to be similarly influential, but no data to support a critical halide content were established.

- For solution temperatures below 175°C, solution flow rate had no effect on corrosion of type 347 stainless steel; at higher temperatures, flow rates of 5–10 m/s were necessary to realize corrosion-erosion effects. Above the critical velocity for accelerated corrosion-erosion, an increasing concentration of uranyl sulfate and/or sulfuric acid acted to increase the relative corrosivity of the solution.

- Results of experiments with van de Graaff electrons revealed no effect of that type of irradiation on corrosion rates; experiments included oxygenated 0.17 M UO_2SO_4 at 250°C at an estimated power density of 25 kw/L adjacent to the specimen, and oxygenated 0.04 M UO_2SO_4 at 280°C at an estimated power density of 60 kw/L adjacent to the specimen. These twin experiments (with and without electron irradiation) in each case yielded no effect on corrosion rate of type 347 stainless steel.

- Results from reactor process experience suggest little effect of ionizing radiation (fission processes) on corrosion of type 347 stainless steel; corrosion was estimated to be 6–8 mil/year based on nickel accumulation in solution (~14 kw/L average power density at positions of uranyl sulfate solution contact with stainless steel and temperatures up to 250–275°C). In addition, no corrosion was detected to be associated with type 347 stainless steel in HRE-2 service (<1 kw/L average power density at positions of uranyl sulfate solution contact with stainless steel and temperatures).

- No significant acceleration of corrosion was observed for type 347 stainless steel specimens exposed at in-pile positions in flow loops, that is, positions in which the specimen itself was not exposed to neutrons but was exposed to the solution that had passed through the core. All corrosion rates were found to be ~2 mil/year at flow rates of 3–12 m/s.

The HRT experience [3] also incorporated a significant amount of data concerning corrosion of zirconium-alloys in uranyl sulfate solutions. As a generality, the zirconium alloys examined were all quite resistant to corrosion and stress-corrosion cracking for temperatures below about 300°C in a wide range of uranyl sulfate and acid concentrations at flow rates up to ~ 5–10 m/s. Some example data appear in Table 4, which shows the corrosion rate of zirconium and Zr-2 in 0.04 M UO_2SO_4 (with other constituents added) as a function of temperature. The data of Table 4 were generated for long-term static autoclave exposure of specimens in the absence of ionizing radiation; and the solution was described as "oxygenated," but a specific amount was not reported. The authors added the observation that these rates were constant or decreasing over exposure times of up to 20,000 h and that similar low corrosion rates were observed for uranyl sulfate concentrations across the range of 0.02 – 0.13 M. Further, deaeration (compared with oxygenated solutions) had little effect on zirconium corrosion below 300°C. It was also observed that, in certain exposure tests in which the containment included stainless steel components in contact with the test fluid, iron and chromium oxides from the stainless steel corrosion process tended to appear in the outer layer of the ZrO_2 layer formed on the zirconium alloys. The latter oxide was found to be brown or brass colored for temperatures less than 250–300°C, and tending toward black for higher-temperature exposures and/or intense ionizing radiation.

Table 4. Corrosion rates for Zr and Zr-2 as a function of temperature in static exposures in oxygenated 0.04 M UO_2SO_4 + 0.02 M H_2SO_4 + 0.005 M $CuSO_4$ without the presence of ionizing radiation

Specimen Material	Corrosion rate (mil/year)		
	200°C	250°C	300°C
Zr	<0.01	<0.01	0.13
Zr-2	<0.01	<0.01	0.04

Data adapted from J. A. Lane, H. G. McPherson, and Frank Maslan, eds, *Fluid Fuel Reactors*, Addison-Wesley, 1958 [3].

Various in-pile flow loops and autoclave experiments were also conducted [3] to examine the potential for acceleration of zirconium corrosion by ionizing radiation. The tests conducted for this purpose were less numerous or systematic than for other situations, but in general the solutions incorporated included 0.17 M UO_2SO_4 with variable excess sulfuric acid and copper sulfate additions, and with overpressures of oxygen and/or radiolytic gases that were not explicitly reported. Power density varied widely (0.3 to 20 kw/L) and temperature was commonly 250–300°C. Results were less "uniform" in nature than equivalent studies for stainless steel exposures. One autoclave experiment result indicated that radiation at any level increased the corrosion of Zr-2 about 100 fold compared with the no-radiation equivalent, but even so the highest corrosion rates observed remained less than 1 mil/year at 250°C. In similar experiments at higher temperatures (250–280°C and power densities up to 20 kw/L), Zr-2 specimens were observed to corrode at rates up to 8 mil/year in all but one extreme case (16 mil/year). No effects of fast electron irradiation (60–90 kw/L) were observed for Zr-2 at 250–300°C. Some differences were detected in the passive films formed on zirconium in-pile compared with out-of-pile equivalents; generally, the in-pile films were darker, contained some uranium, and were easier to remove than films formed out-of-pile. Further, Zr and Zr-15Nb were found to behave similarly to Zr-2.

In summary, past experience associated with the Homogenous Reactor work suggests that zirconium-based alloys and stainless steels of composition similar to type 347 are expected to exhibit only very modest corrosion for the conditions expected within the SHINE process, which generally encompasses lower temperatures, flow rates, and radiation loads than experienced by materials tested/used in the HRT work.

Separate from the discussion of corrosion in uranyl sulfate solutions, it is important to recognize that the SHINE process conditions expect to use a slight excess of sulfuric acid (~0.1 M) primarily to maximize the solubility of uranium species. Although this concept was included in much of the HRT work to examine corrosion of containment materials, it remains particularly relevant to the selection of superior stainless steel materials for the SHINE process piping. At issue is that sulfuric acid is generally quite corrosive to most austenitic stainless steels—at least above particular alloy-dependent temperatures and concentrations—which are best employed in electrochemically oxidizing conditions. As a result, some awareness of this potential sensitivity may improve material selection for the SHINE system piping components. To that end, handbook style literature was examined for indications of "boundaries" associated with potentially excessive corrosion of stainless steels in solutions bearing sulfuric acid.

In summary, the available information indicates—all other things equal—that stainless steels containing a modest amount of Mo (2–4%) are resistant to dilute sulfuric acid over a much wider concentration and temperature range than equivalent stainless steels with little or no Mo in the composition. Perhaps the best and most straightforward example is the comparison between 304L (nominally contains no intentional Mo addition), 316L (2–3% Mo), and 317 (3–4% Mo) stainless steels, all of which are widely used in the chemical processing industries. They are very similar in general composition (Table 2 offers a partial comparison) but are distinguished for corrosion resistance primarily by the relative Mo content. The presence of 2–4% Mo provides increased resistance to the reducing environment (meaning relatively

low electrochemical potential) generated by sulfuric acid solutions via improvement of passive film stability, particularly for relatively dilute solutions. Various handbooks and corrosion data compendiums are replete with examples indicating this trend, and two specific illustrations have been adapted below. Figure 1 compares corrosion rates reported for 304, 316, and 317 stainless steels in a series of 20°C corrosion tests as a function of concentration of sulfuric acid in water. These data suggest that, across a wide range of acid concentration, 2–4% Mo in 316/317 reduces the corrosion rate by approximately an order of magnitude compared with the corrosion rate indicated for 304 stainless steel.

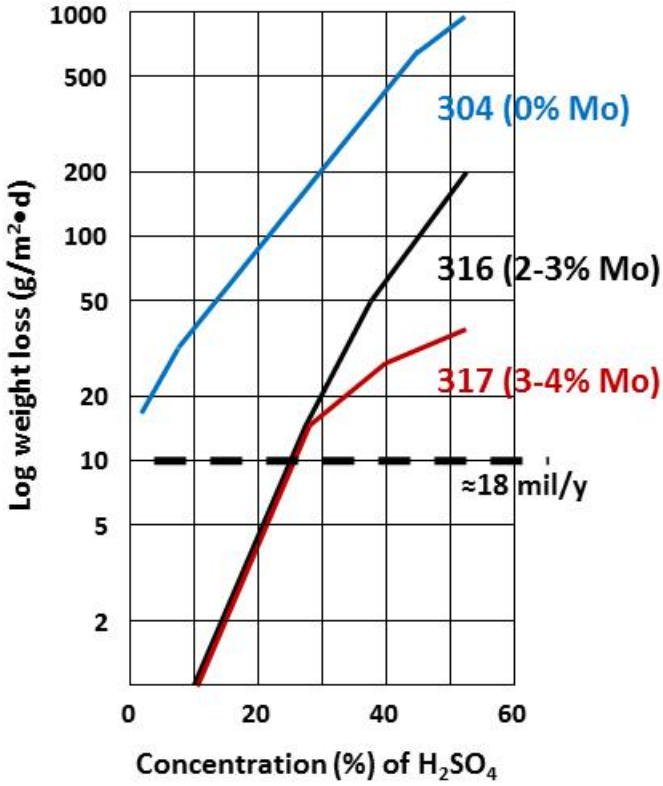

Fig. 1. Corrosion rates of stainless alloys at 20°C as a function of sulfuric acid concentration in water. The state of aeration for the sulfuric acid solutions was not recorded in Ref. 6, from which the data were adapted, but it seems likely that the solutions were naturally aerated; that is, there was no intentional control of oxygen content. For ease of conversion to more common corrosion rate units, note that 10 g/m^2-d corresponds to approximately 18 mil/year.

Even at the relatively low sulfuric acid concentration anticipated in the SHINE process (on the order of 1%), there appears to be a potential advantage to selection of 316 stainless steel over type 304. Figure 2 shows that the potential advantage of modest Mo content extends across a range of temperatures relevant to the SHINE process.

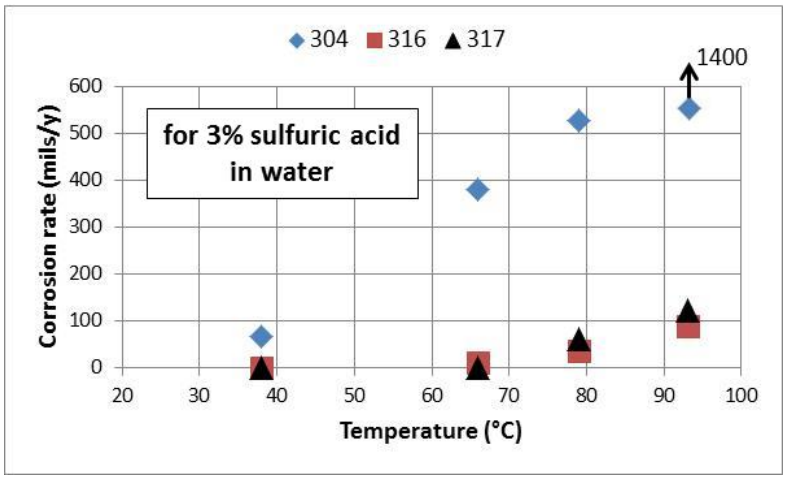

Fig. 2. Corrosion rate of austenitic stainless steels as a function of temperature in 3% sulfuric acid (in water). The state of aeration for the sulfuric acid solutions was not recorded in Ref. 7, from which the data were adapted, but it seems likely that the solutions were naturally aerated; that is, there was no intentional control of oxygen content.

3. EXPERIMENTAL PROCEDURE

3.1 LABORATORY TESTING WITH DEPLETED URANIUM

3.1.1 Corrosion Test Environments

In discussions with SHINE personnel, a set of laboratory test conditions was identified to represent the chemical process conditions routinely expected within the target solution vessel (zirconium-based material) and the process piping and columns (stainless steel). In addition to the "baseline" conditions expected for each major process variable, a range around the expected nominal condition was also selected for study. Exclusive of any chemistry perturbations caused by radiolysis, the baseline conditions and relevant ranges selected included the following.

a) Nominal concentration of 140 g/L depleted uranium in solution; range of 70–280 g/L

To prepare baseline solutions, reagent-grade depleted uranyl sulfate trihydrate ($UO_2SO_4 \cdot 3H_2O$) was purchased from a commercial supplier in coarse powder form and added to reagent-grade water in appropriate amounts. The certificate accompanying the trihydrate material claimed 99.9% purity, with a total insoluble matter content of < 0.005%. Chlorides, iron, and heavy metals (as lead) were all reported as < 0.002%, and other sulfates (alkali metals and alkali earths) at less than 0.05%. At 420.1 g/m for the trihydrate, the uranium fraction of this material was about 56.7%; thus 246.9 g of trihydrate per liter of water was required to achieve 140 g dU/L. The sulfate was readily soluble in room-temperature water across the entire range of solute concentrations selected, generating a bright yellow solution and a slight volume increase (~40–100 ml per liter, depending on concentration) resulting from the solid addition.

It should be noted that the addition of 246.9 g of trihydrate to 1000 ml of water to prepare an intended solution of 140 g dU/L generated a final solution volume of about 1060 ml. In reporting of test solution concentrations, this minor deviation (about 6% on average across all the different solution concentrations employed) was not incorporated. Thus the precise concentration of dU/L in these tests is slightly less than the target value as a result of this increase in solution volume. As will be shown, however, corrosion

was not sensitive to uranyl sulfate concentration over a very wide range, so this factor has no practical consequence.

b) Nominal excess sulfuric acid concentration of 0.1 M; range of 0.01–1.0 M

Although the nominal solution of 140 g dU/L is quite acidic (pH ~ 0.8), a small excess of sulfuric acid will be added in the SHINE process to ensure the complete/stable solubility of the uranium during processing. Reagent-grade sulfuric acid (density = 1.84 g/ml, 98.08 g/m, ~ 17.8 M) was used to make these additions, which corresponded to about 5.6 ml of reagent acid added to 1 L of solution for the nominal solution strength of 0.1 M excess acid.

c) Nominal fluid temperature of 65°C; range of 65-94°C

As a generality, the circulating process solution is expected to be ~65°C in a range of locations throughout the process. Some separation columns are expected to experience temperatures near 80°C. As a method to accelerate potential corrosion issues and consider the consequences of process upsets that involve a temperature increase, the upper bound for test temperatures was set at 94°C. This temperature was the maximum stable value in the constant-temperature bath used for these exposures.

d) Nominal iodine species concentration ≤ 1 wppm; range 0-50 wppm

There is some expectation that a trace amount of iodine species will be formed as a result of the fission process in the target solution. Model calculations at SHINE [8] suggest that normal concentrations of iodine will likely be less than 0.1 wppm, but that iodine might approach levels near 1 ppm if the solution is reused sufficiently and/or the uranium extraction process is used infrequently. However, the ^{99}Mo extraction column also removes some iodine, so 1 ppm seems a realistic upper limit on halide contamination. The form of the iodine (I^-, IO_3^-, etc.) however, is not known with certainty. Thus higher concentrations of iodine species were periodically incorporated as a method to accelerate potential corrosion effects and assess sensitivity to this variable. Iodine species were added to test solutions via reagent-grade KI and reagent-grade KIO_3 in roughly equal amounts to reach the target iodine concentration. For example, for a target concentration of 10 wppm iodine, sufficient KI and KIO_3 were added that roughly 5 wppm I^- and 5 wppm I^- as IO_3^- were included. These additions were prepared by weighing very small quantities of solid (as small granules) for additions, and there is thus some error anticipated in the reported wppm values (perhaps ± 2 wppm).

e) Oxygenation level not specified

The SHINE process does not plan to specifically influence the oxygen content of the process solution. However, a crude attempt to consider relative oxygenation incorporated test exposures of coupons fully immersed in solutions of interest, as well as exposed within the condensing vapor immediately above the same solutions. Naturally aerated solutions were used as starting stock, but no attempt was made to buffer the solution to a constant oxygen level; so it is possible that oxygen content could be altered/consumed during prolonged exposure within the liquid. In contrast, slight in-leakage of air into the vapor space of the test vessels is likely to ensure saturation of the very thin films of liquid on the specimen surfaces in the vapor space.

f) Nominal flow rate relatively low but not specified

Compared with the high fluid velocities required to generate significant erosion–corrosion issues (on the order of 5–10 m/s) as reported in the Literature Review, the flow rates expected in the SHINE process are expected to be very modest (approximately an order of magnitude lower). As a result, it was decided that

static testing would suffice for most exposures in this preliminary assessment. Fluid flow rates approaching 10 m/s via pumping mechanisms are problematic in the laboratory because of space limitations and health/safety restrictions on pressurized radioactive fluids; therefore, limited testing of velocity effects will be considered using alternate methods to be discussed in subsequent sections.

g) Unknown/unspecified radiolysis products in solution

Water tends to be decomposed by all types of high-energy radiation to yield predominantly hydrogen, oxygen, and hydrogen peroxide as well as perhaps several radicals formed from these constituents. Such radiolytic activity is expected within the SHINE process solution. Some of these radicals are very short-lived (unstable) and recombine to form water before they can diffuse throughout the aqueous system to influence chemistry and other reactions. Typically, the net oxidation/reduction tendency that results from radiolysis depends upon the amount and action of the hydrogen peroxide formed [3]. The peroxide may act either way (depending on the overall oxidation-reduction potentials within the system), but usually oxidation is favored. In the presence of oxygen, H atoms may also be converted to HO_2, which also acts as an oxidizing agent [3]. No specific information regarding the concentrations and longevity of any radiolysis products expected within the SHINE system was available to guide the initial corrosion testing; therefore, nitric acid, a strong oxidizing agent, was added in modest amounts to test solutions as a "simulant" of oxydizing radiolysis products. Reagent-grade nitric acid (density = 1.413 g/ml, 63.01 g/m, 15.7 M) was used in each case, aiming for up to 0.25 M nitric acid. Electrochemically reducing potentials resulting from radiolysis products were incorporated, albeit indirectly, via large sulfuric acid additions as previously mentioned.

3.1.2 Corrosion Test Materials

At the time the corrosion testing program was initiated, two zirconium-based alloys that were candidate materials for the target solution vessel—Zircaloy 4 (hereafter designated Zr-4) and Zr-2.5Nb (ZrNb)—were already part of a program at ORNL tasked with examining radiation damage properties associated with anticipated SHINE neutron exposures. The studies included exposures of specimens in the High Flux Isotope Reactor (HFIR) and incorporated intentionally hydrided specimens, among many other conditions.

At the outset of the corrosion program, two stainless steels had already been selected as candidate materials for balance-of-plant process piping. Among them, austenitic 316L stainless steel is very common to the chemical process industry and has well-documented corrosion resistance in a wide variety of environments. The much less common type 2304 duplex stainless steel was also under consideration primarily for the higher strength (~ 2×) it offers, albeit at a higher price than 316L. These two alloys were included in all of the corrosion exposures. In addition, included in select exposures within the program were two other stainless steels. Type 304L stainless steel represents less expensive but perhaps more widely available (in a variety of sizes and forms) material than 316L, but it has somewhat less corrosion resistance in the sulfuric acid–oriented environments expected in the SHINE process. Type 17-4 PH stainless steel (also referred to as type 630 stainless steel), a precipitation-hardenable grade, was included because there is some consideration of using it for compression fittings between process pipes to minimize welding requirements in fabrication. The radiation damage for the stainless steel process piping is expected to be generally much less intense than for the target solution vessel; but lack of literature data—which are generally available for 316L and 304L—caused type 2304 to be included in the radiation damage assessments of a separate task.

Thus the corrosion assessments focused on these candidate alloys previously identified by SHINE personnel. Table 5 shows the composition of each stainless alloy and Table 6 the composition of the zirconium-based alloys. All the stainless steels were evaluated for corrosion resistance in the mill-

annealed condition; the Zr-4 was examined in the alpha-annealed condition, and the ZrNb was studied in the beta-quenched condition.

Table 5. Composition (wt %) for stainless steel alloys. Data from 316L and 2304 from sample test report; 304L and 17-4 PH from mill certification. Note the carbon content of the 304L was actually slightly higher than the "L" grade maximum of 0.030, but this was not noticed until specimens were already machined

Element	Stainless type			
	316L	**304L**	**2304**	**17-4 PH**
Fe	bal	bal	bal	bal
Cr	17.04	18.36	23.85	15.21
Ni	10.97	8.22	4.53	4.17
Mo	2.02	–	0.24	0.13
Mn	1.40	0.89	1.30	0.49
Si	0.38	0.35	0.42	0.44
P	0.031	0.032	0.030	0.025
S	0.014	0.001	0.003	0.001
C	0.026	0.041	0.028	0.04
N	0.02	0.04	0.10	0.03
Cu	0.19	–	0.24	3.38
Nb	–	–	–	0.32
V	0.03	–	0.04	–
W	–	–	0.07	–
Co	0.13	–	0.08	–

Table 6. Composition (wt %) for zirconium-based alloys. Data from the mill certification for the original ingot before processing. No other elements were detected in concentrations above 30 wppm. Alloys obtained from ATI Specialty Alloys in Albany, OR.

Element	Zr-4	Zr-2.5Nb
Zr	bal	bal
Cr	0.11	–
Fe	0.20	0.10
Sn	1.52	–
Nb	–	2.58
O	0.15	0.09
C	0.014	–

For most exposures, the specimens were 30 × 19 × 3 mm (14.6 cm^2 surface area). They were tested originally in the as-machined condition (average roughness ~ 16 micro-inches) and, when specimens were reused, were lightly ground with 240 grit paper. For galvanic corrosion testing, the same coupons were used with a 9.5 mm (⅜ in.) hole placed in the center (for the stainless steel bolt and Teflon shoulder washers). For cavitation testing (described in a subsequent section), different plates of the stainless steels were used to make the specimens; but the compositional differences between these test results and the values listed in Table 5 were trivial.

3.1.3 Corrosion Test Methods

a) Static immersion testing

Specimens were exposed to the environment of interest within wide-mouth Erlenmeyer flasks fitted with cold-finger condensers. Approximately 25°C water was circulated through the condensers, which fit snuggly in the top of each flask, to eliminate evaporation and maintain constant solution composition. Each flask contained up to three small glass specimen "trees" that cradled up to three specimens each so that contact between specimen and glass was reproducibly minimized. The flasks, filled with solution and specimen trees, were placed within a constant-temperature bath as shown in Fig. 3. The bath comfortably held four such flask arrangements, with cooling water for the condensers flowing in series among the cold-fingers from a recirculator. After the flasks were placed within the bath with cold-finger condensers in place, hollow plastic beads about 1.5 cm in diameter were added to the bath surface to provide 5–6 cm of insulation and evaporation deterrent for the water within the bath. At the top of the water bath, a plastic lid with an opening for each flask was pressed into place to further limit evaporation. In addition to the temperature feedback provided electronically from the water bath, two additional thermometers (one digital, one analog) were used to further monitor and confirm the test temperature. The test temperatures remained constant (± 0.5°C) indefinitely at the desired value, except for ~5 minute excursions to temperatures ~10°C below the set point when additional water was added to the tank for the highest-temperature exposures. (Water evaporation from the bath was reduced but not eliminated by the plastic beads and lid.)

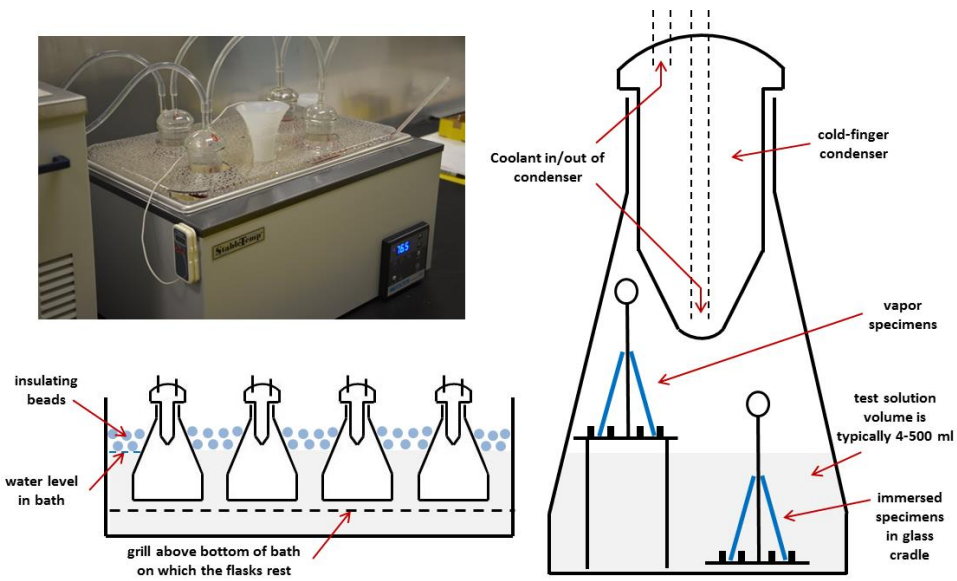

Fig. 3. Photograph of water bath during testing (upper left) and schematic drawings of flask placement within the water bath and specimen placement within a flask.

Although the solution temperature was equal to that of the immersed specimens during testing, the temperature associated with the specimens exposed in the vapor phase was less certain. The glass trees holding the vapor specimens were intentionally sized to position the specimens just barely above the fluid level (in some tests, a small corner of the coupon was actually wetted by liquid), but a temperature gradient is assumed to exist in the vapor above the solution because of the proximity of the cold-finger condenser. It seems likely that the average temperature of the vapor-phase coupons was on the order of 5–10°C below that of the liquid, as was confirmed by a film of condensed liquid; but no measurements were made to support that estimate. Some effort was made to avoid placing a vapor specimen tree

directly beneath the condenser tip to avoid constant "washing" of the specimens via dripping condensate, but it is not possible to say that periodic dripping from the condenser onto specimens did not periodically occur.

Static immersion testing routinely consisted of 96–100 h exposures of specimens at the selected conditions. Following the exposure period, specimens were briefly rinsed in deionized water and wiped dry with a paper towel. Subsequently, they were ultrasonically cleaned in acetone for ~5 minutes and again wiped with a paper towel. They were then weighed (using a scale capable of ± 0.05 mg) and—using the exposure time, exposed surface area, and material density—the total mass loss was used to calculate an annual uniform corrosion rate. In most instances, no corrosion product (e.g., discoloration of the white paper towel) was detected to be associated with the specimen cleaning process, although there are exceptions (as discussed in the Sect. 4, Results).

b) Planned-interval testing

As a special subset of the static immersion testing, a more detailed examination of corrosion rates as a function of time was incorporated on a limited basis using the "planned-interval" protocol described in ASTM G31 [9]. In this method, identical coupons of a material are exposed for preselected units of time in a test solution that is not changed or significantly replenished over the course of the experiment. Figure 4 is a schematic diagram representing the planned-interval test methodology. In principle, the standard unit of time for exposure in the test can be any convenient/appropriate duration; in the present experiment, it was set at 2 days. Thus the total duration of the experiment was 8 days (192 h).

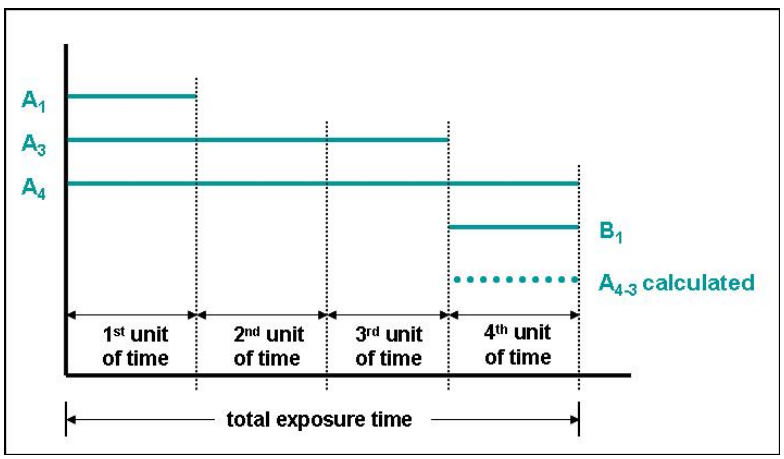

Fig. 4. Schematic diagram of the planned-interval test strategy. The subscript for each label refers to the number of units of time in the exposure.

At the beginning of the experiment (time = zero on the abscissa in Fig. 4), three sets of coupons were exposed in the freshly prepared test solution. At the end of the first unit of exposure time (here, 2 days), one set of coupons (A1) was removed from the test for evaluation. Another set of coupons (A3) was removed from the experiment at the end of the third unit of time (6 days of exposure). At the same time as the A3 coupons were removed, a fresh set of coupons (B1) was added to the test for the final 2 days of exposure. At the end of 8 days, all remaining coupons (A4 and B1) were removed from the test environment for evaluation. In all cases, post-exposure evaluation included an assessment of the appearance (e.g., corrosion films and discoloration, evidence of pitting) and weight change following cleaning as previously described.

A primary advantage of the planned-interval test protocol is that specimens are included or removed in a pattern that allows the experimenter to calculate general corrosion rates (or other changes) as a function of

exposure time and to distinguish potential changes in compatibility associated with liquid corrosivity and corrodibility of the metal. For example, by comparing the weight change experienced by fresh coupons exposed only in the initial 2 days (A1) and the final 2 days (B1), potential changes in the aggressiveness of the test environment in the intervening time can be assessed. Among many possibilities, a much lower apparent corrosion rate in the final unit of exposure time (B1) compared with the same duration exposure at the outset of the test (A1) might signify that an aggressive constituent of the test environment was consumed during testing, rendering the environment relatively more benign with time. Alternatively, a higher corrosion rate at the end of the test (B1) might suggest that corrosion products have accumulated, leading to a more corrosive environment, or that something has entered the environment over time (e.g., in-leakage of air) to cause the corrosivity to increase.

Assessment of the corrodibility of the metal as a function of time is also a part of the planned-interval strategy. By comparing the weight change of specimens exposed for four units of time (A4) and three units of time (A3), a virtual coupon exposure representing the increment of corrosion occurring between three and four units of exposure (A4-3) can be calculated. This virtual exposure result represents corrosion in a single unit of time but for a coupon surface that is not fresh. By comparing the virtual result (A4-3) with the result for the same single unit of time but on a fresh surface (B1), the influence of the surface condition can be evaluated. For example, a calculated weight loss for A4-3 that is significantly less than the value observed for B1 suggests that a passive film or corrosion layer has formed that tends to inhibit subsequent corrosion. Alternatively, a weight loss for A4-3 that is higher than for B1 suggests, for example, that the initial air-formed film on coupons is protective for some period of time but begins to fail upon extended exposure.

The planned-interval strategy was used primarily to examine potential effects associated with iodine species in solution. For most materials, experiments included both full immersion and coupons exposed in the vapor phase above the solution of interest.

c) Galvanic corrosion testing

Identical specimens to those used in immersion testing were used for the galvanic couple exposures, except that the latter incorporated central holes (~ 9.5 mm diameter) to accommodate the spacers and hardware, as depicted in Fig. 5. Specimens were mechanically pressed together by the flattening action of the lock washer so that the resistance across any given pair of specimens was ≤ 0.2 ohms. This was identical to the resistance measured from end to end of the threaded bolt. Teflon shoulder washers were used to eliminate electrical contact between any of the specimens and the stainless steel hardware, ensuring that the specimens contacted only one another.

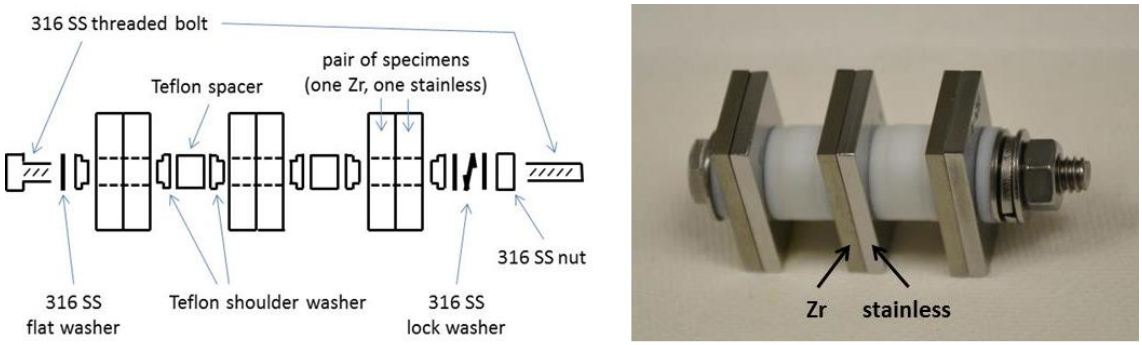

Fig. 5. Schematic diagram of an assembly with three pairs of potential galvanic couples (left) and an actual assembly (right).

In all cases, the galvanic couples consisted of a zirconium alloy (Zr-4 or Zr-2.5Nb) coupled with a stainless steel (316L, 2304, or 17-4 PH). Typically, three mutually isolated couples were tested together on one stainless steel bolt, which was fully immersed in the test solution of interest for ~72 h. Following the exposure, the assembly was dismantled for cleaning and weighing of the individual specimens as described previously. In cases of very little or no observable corrosion and/or weight change, the specimens were reused in the next galvanic test exposure with no additional surface preparation. In cases of more substantial film formation or corrosion, the specimens were lightly ground on 240 grit sandpaper and reweighed before further testing.

d) Vibratory horn testing

One finding from the HRT/HRE data previously reviewed is that, at sufficiently high uranyl sulfate temperatures and velocities, a considerable erosion/corrosion component was introduced into material compatibility considerations. The critical fluid velocity, on the order of 10 m/s above 175°C, was very much greater than the velocity expected at any location within the SHINE process vessels and piping. Furthermore, no serious elbows or fluid pressure changes are planned/designed that could introduce cavitation in the process fluid. Thus erosion/corrosion features are not anticipated in any component of the SHINE process. However, to gain insight into potential differences in sensitivity to this factor among the candidate alloys, cavitation testing using a vibratory horn was incorporated into the test plan (meeting the intent of the protocol described in ASTM G32 [10]).

Figure 6 shows the key components of the vibratory horn (fabricated using titanium) and a schematic diagram of a test specimen that mounts to the tip of the horn. Each vibratory horn was tuned for a specific specimen weight range (which for this size horn was ~ 5–8 g). Thus, to account for different densities among the various test materials, the dimension "h" shown in Fig. 6 was varied to maintain a near-constant mass for each test specimen.

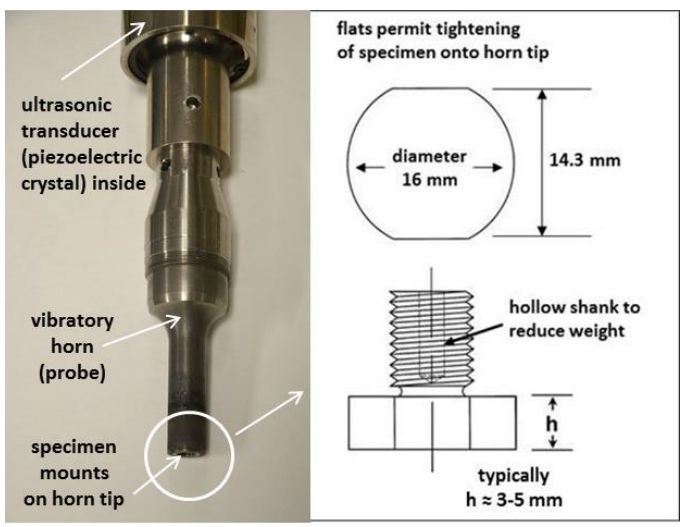

Fig. 6. Key components of a vibratory horn (left) and details of a cavitation test specimen (right).

Figure 7 depicts a specimen mounted to the end of the vibratory horn and partially immersed (by about 2 mm) into the test solution of interest. In this case, the fluid container was a jacketed glass vessel that permitted temperature control of the test solution via circulation of water from a constant-temperature bath maintained at 23°C in this round of testing. Each test specimen had a surface area of 180 mm^2 exposed to cavitation conditions (the flat surface perpendicular to the major horn axis). In all cases, the horn tip oscillated at a fixed frequency of 20 kHz and was set to generate a peak-to-peak vibrational

amplitude of 25 µm. The rapid reciprocating displacement of the specimen surface at the horn tip induced the formation and collapse of cavities in the liquid near the specimen surface. The damage can be quantified and compared via weight loss or, in sufficiently aggressive cases, pit depth. Each exposure in the present testing included 10 s of sonication followed by a pause of 10 s to permit corrosion or (re)passivation to occur after disruption of the normally passive film.

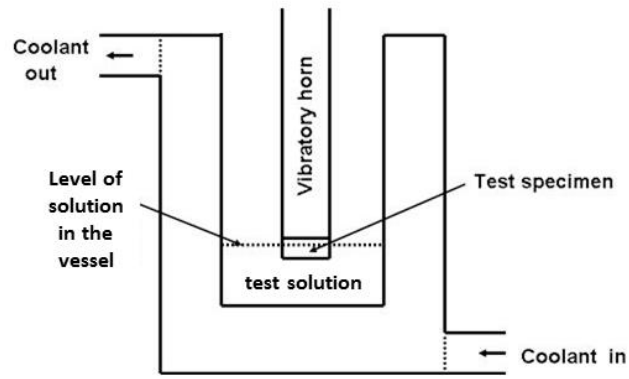

Fig. 7. Schematic diagram of the cavitation test container and relationship to horn/specimen. The test solution of 100 ml was confined in a volume of about 5.5 cm diameter and a fluid depth of about 4 cm.

At 1 h intervals (30 min "on" and 30 min "off" of sonication), specimens were ultrasonically cleaned sequentially in distilled water and acetone, with each process followed by light wiping with a fresh paper towel. Mass change and observations of the test surfaces as a function of sonication time were recorded.

A test solution containing 140 g dU/L (made with depleted uranyl sulfate trihydrate) with 0.1M excess sulfuric acid added (baseline SHINE composition) was used in one exposure campaign. In the other, sodium sulfate (Na_2SO_4) was used instead of uranyl sulfate to eliminate the uranium component of the solution. Solutions of sodium sulfate tend to be slightly basic, so the addition of relatively more sulfuric acid was required to generate a pH similar to that of the uranyl sulfate (about 0.8). The density of the uranium-free solution was slightly less than that of the uranium-bearing solution (about 1.06 vs 1.16 g/cm^3).

e) Corrosion testing with irradiation conditions

Small containers (316L stainless steel) were prepared for exposure of a limited number of coupons with a limited volume of uranyl sulfate solution in the spent fuel pool at HFIR. They were exposed in the Gamma Irradiation Facility (GIF), an area designed specifically for material assessments. The container and specimens are depicted schematically in Fig. 8. Conceptually, those containers (with internal dimensions of approximately 5 cm in diameter and 9 cm in height) would be loaded into previously approved/certified canisters for insertion into GIF within a spent fuel bundle. They would be about half filled, with about 60 ml of uranyl sulfate solution, to permit specimen exposures as immersed and in vapor. Depending on the burnup and age of the fuel (i.e., cooling time in the pool), exposures of different gamma intensity (and resulting equilibrium temperature) can be selected based upon position in the pool. Further, different gamma intensities can be selected by the relative vertical position of the small container within the larger/taller canister, as suggested by the right side of Fig. 8. At the end of FY 2014, final safety approvals for the individual test containers (modified from Fig. 8 to incorporate redundant pressure relief values) had been completed. Test exposures of containers containing water only, no specimens or uranyl sulfate, were being prepared to examine gamma intensity and the potential temperature rise of the internal liquid as functions of a few positions within the pool. Actual testing of specimens and active solutions is planned for the early part of FY 2015.

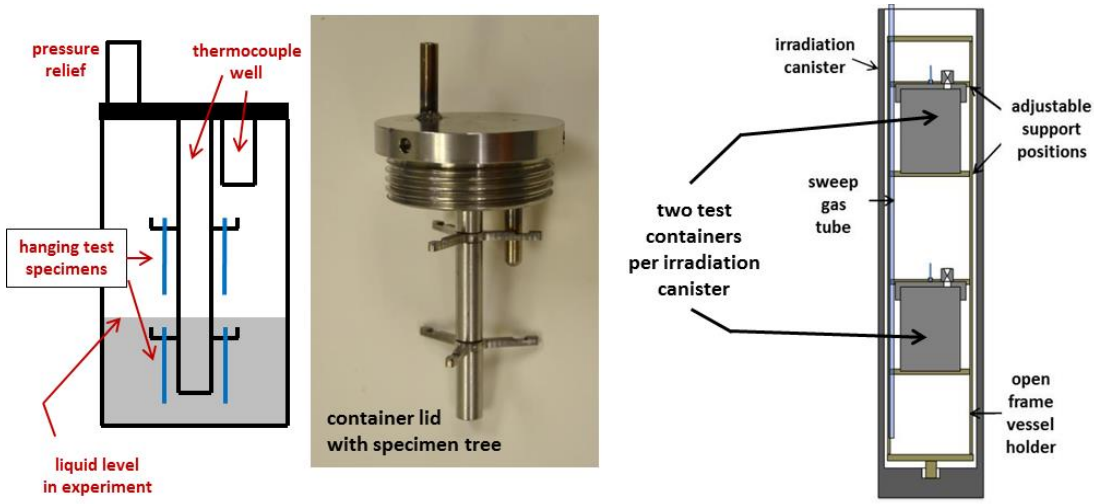

Fig. 8. Schematic diagram of an irradiation test vessel (left) along with an actual container lid with various attachments shown. At right is a schematic diagram of the full-size irradiation canister containing two test vessels, showing that the relative position of the internal vessels can be adjusted. For scale, note that the individual test vessels are about 11 cm tall in external dimension, exclusive of pressure relief valves.

4. RESULTS AND DISCUSSION

Initial testing focused on static exposures in a range of solutions representing the expected SHINE conditions and incorporated only the zirconium alloys (Zr-4 and ZrNb) and the two primary stainless steels (316L and 2304). As the testing progressed, two other stainless steels (304L and 17-4 PH) were added to selected exposures. In addition, as testing proceeded and very low corrosion rates were routinely determined, exposures tended to focus on only the highest-temperature exposures to potentially accelerate or intensify the meager reactions observed.

Table 7 summarizes the corrosion test results from the initial testing in the baseline depleted uranyl sulfate concentration corresponding to 140 g dU/L. The results from these static exposures generated consistently miniscule corrosion rates for the zirconium alloys and the primary stainless steels (316L and 2304), with no calculated corrosion rates above 0.07 mil/year for any of these alloys. Types 304L and 17-4 PH stainless steels were included in the exposures at the highest temperature. These experienced somewhat higher corrosion rates than the other materials but, in all cases, exhibited rates of less than about 0.4 mil/year.

Following the static exposures outlined here, the zirconium alloys were generally found to exhibit a uniform, very light golden-brown discoloration that tended to become darker brown as the exposure conditions became more aggressive (higher exposure temperature and/or higher uranyl sulfate concentration). As a trend, specimens exposed at 65°C (immersed or in vapor) did not exhibit readily visible discoloration; but at exposures ≥80°C, discoloration was routine on immersed specimens and perhaps slightly less intense on specimens exposed in the vapor. Figure 9 presents a representative observation for the range of discoloration observed on Zr-4 specimens (which, to the unaided eye, were identical to Zr-Nb specimens).

Table 7. Corrosion rates calculated from weight change for specimens exposed in uranyl sulfate corresponding to a concentration of 140 g dU/L, as a function of excess acid addition and temperature. At the bottom of the table, ambient pH values are indicated for the initial solution mixture and the range of values observed at intervals during the ~96 h exposures

		-- -- -- -- Corrosion rate calculated from weight loss, mil/y -- -- -- --								
in 140 g dU/L		temperature = 65-66˚C			temperature = 80-81˚C			temperature = 93-94˚C		
		excess sulfuric acid concentration			excess sulfuric acid concentration			excess sulfuric acid concentration		
specimen	location	0.01 M	0.10 M	0.25 M	0.01 M	0.10 M	0.25 M	0.01 M	0.10 M	0.25 M
Zr-4	immersed	0.05	0.00	0.00	0.03	0.00	0.03	0.00	0.04	0.00
Zr-4	vapor	0.03	0.00	0.01	0.01	0.02	0.00	0.00	0.02	0.00
ZrNb	immersed	0.05	0.00	0.02	0.00	0.00	0.03	0.00	0.00	0.00
ZrNb	vapor	0.00	0.00	0.00	0.02	0.01	0.01	0.00	0.01	0.00
316L	immersed	0.03	0.00	0.00	0.02	0.00	0.03	0.04	0.02	0.00
316L	vapor		0.00	0.02	0.00	0.02	0.05	0.02	0.01	0.00
2304	immersed	0.03	0.02	0.00	0.00	0.06	0.03	0.02	0.01	0.00
2304	vapor		0.07	0.03	0.02	0.01	0.01	0.01	0.03	0.00
304L	immersed							0.26	0.05	0.06
304L	vapor							0.14	0.06	0.11
17-4 PH	immersed							0.17	0.18	0.41
17-4 PH	vapor							0.06	0.00	0.07
initial pH observed		0.78	0.48	0.45	0.84	0.65	0.38	0.76	0.66	0.54
pH range		0.77 - 0.80	0.48 - 0.63	0.45 - 0.52	0.82 - 0.97	0.61 - 0.66	0.38 - 0.47	0.73 - 0.87	0.55 - 0.75	0.39 - 0.59

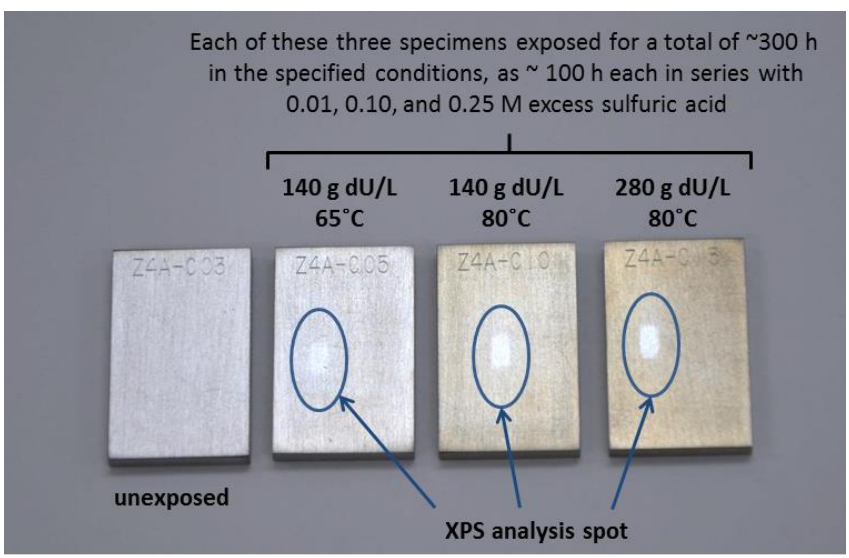

Fig. 9. Range of discoloration observed on Zr-4 specimens as a function of the indicated exposure conditions. X-ray photoelectron spectroscopy was used to examine the surface film composition on the exposed specimen. The brown coloration of the Zr-4 specimens is subtle, and the overall contrast in the photo was manipulated to enhance the apparent gradation of color.

X-ray photoelectron spectroscopy (XPS) was used to examine the composition of the film formed on each of the exposed alloys shown in Fig. 9. In all cases, most of the film was found to be ZrO_2 of a thickness that increased from 17 to 24 to 26 nm as the brown discoloration intensified. Note that in Fig. 9, the relative intensity of the brown discoloration can also be readily observed by comparing the luster of the

analysis spot, from which the entire film has been sputtered away, with the remainder of the adjacent surface. As the film became darker, it was observed that the amount of tin (as SnO) in/on the outer layer (~5 nm) of the film increased proportionately, from 0.2 to 3.9 to 6.1 at. % as the darkness of the film increased. It is suspected that this increase in tin was a result of the corrosion process upon initial exposure of the alloy (more aggressive solution = more corrosion = more tin). However, the tin was not uniquely responsible for the brown discoloration, as the Zr-Nb were identically colored but contained no tin. Also, as the degree of discoloration increased, slightly more uranium—from 0.03 to 0.26 to 0.46 at. %—was found in/on the surface (~5 nm) film. However, no indication of radioactivity could be detected in standard heath physics smears of any surface, and standard scans for β and γ activity levels on contact were unchanged from background measurements in the laboratory. As suggested by Fig. 9, in all cases the brownish film was sufficiently thin that the original machining marks on the specimen surface remained visible after exposure. The surfaces were completely smooth and free of any localized indications of corrosion, such as pits or other blemishes. For the primary stainless steels under investigation (316L and 2304), the exposures represented in Table 7 resulted in no visibly detectable changes. That is, the specimens exhibited no discoloration or substantial change in luster and, as for the zirconium alloys, the original machining marks and surface quality were undisturbed.

The 17-4 PH specimens immersed at 94°C (see Table 7) were discolored to a deep gun blue or almost black hue (very adherent), whereas the equivalent specimen exposed in the vapor was only discolored in isolated spots. In the latter case, the spots were thought to represent locations at which specimen contact with the glass specimen tree tended to collect condensate and thus simulate an immersion environment. The 304L specimens similarly exposed tended to lose luster but experienced no significant discoloration. In both cases, corrosion attack was sufficiently minor that the original machining marks on both alloys visually appeared to be undisturbed. Figure 10 is representative of these observations.

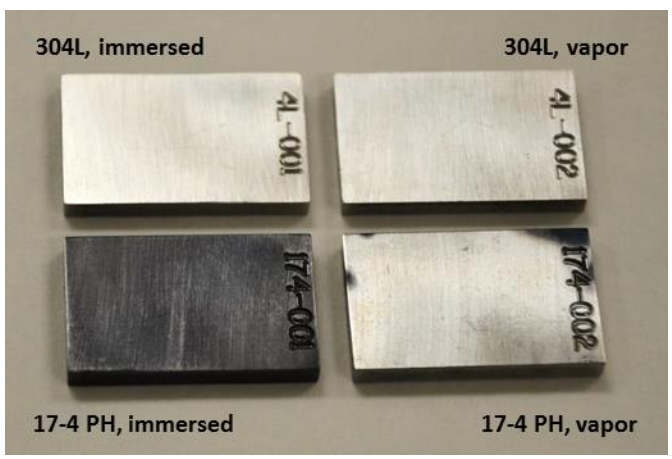

Fig. 10. Surfaces of 304L and 17-4 PH specimens following exposure at 94°C in uranyl sulfate at a concentration corresponding to 140 g dU/L and 0.25 M excess sulfuric acid.

At the bottom of Table 7, the ambient pH values for the as-mixed solution, as well as the pH range at intervals during the ~ 96–100 h exposures are reported. No systematic drift in pH during the exposures was identified. The pH of the uranyl sulfate solution without any excess acid was approximately 0.8, and the pH values were influenced as indicated by the excess acid addition.

Tables 8 (70 g dU/L) and 9 (280 g dU/L) report corrosion rate data for other concentrations of uranyl sulfate examined. It is clear that the corrosion rate of the candidate alloys is not a significant function of the uranyl sulfate concentration or excess sulfuric acid across the range examined. In all cases, corrosion

rates were found to be < 0.1 mil/year, with resulting coupon surfaces as described previously for the 140 g dU/L concentration.

Table 8. Corrosion rates calculated from weight change for specimens exposed in uranyl sulfate corresponding to a concentration of 70 g dU/L as a function of excess acid addition and temperature. At the bottom of the table, ambient pH values are indicated for the initial solution mixture and the range of values observed at intervals during the ~96 h exposures

		-- -- -- -- Corrosion rate calculated from weight loss, mil/y -- -- -- --								
in 70 g dU/L		temperature = 65-66˚C			temperature = 80-81˚C			temperature = 93-94˚C		
		excess sulfuric acid concentration			excess sulfuric acid concentration			excess sulfuric acid concentration		
specimen	location	0.01 M	0.10 M	0.25 M	0.01 M	0.10 M	0.25 M	0.01 M	0.10 M	0.25 M
Zr-4	immersed	0.08	0.02	0.01	0.04	0.04	0.01	0.03	0.02	0.00
Zr-4	vapor	0.03	0.03	0.00	0.00	0.03	0.04	0.00	0.00	0.00
ZrNb	immersed	0.01	0.00	0.02	0.00	0.03	0.02	0.00	0.02	0.00
ZrNb	vapor	0.00	0.00	0.00	0.00	0.03	0.02	0.00	0.00	0.00
316L	immersed	0.01	0.02	0.01	0.02	0.02	0.01	0.03	0.00	0.00
316L	vapor		0.00	0.00	0.01	0.01	0.02	0.02	0.00	0.00
2304	immersed	0.09	0.00	0.07	0.03	0.04	0.00	0.00	0.02	0.01
2304	vapor		0.00	0.00	0.00	0.02	0.00			
initial pH observed		1.03	0.67	0.60	1.03	0.79	0.45	0.68	0.54	0.35
pH range		0.92 - 1.03	0.64 - 0.67	0.60 - 0.68	1.03 - 1.09	0.72 - 0.86	0.42 - 0.51	0.59 - 0.71	0.46 - 0.54	0.30 - 0.35

Table 9. Corrosion rates calculated from weight change for specimens exposed in uranyl sulfate corresponding to a concentration of 280 g dU/L as a function of excess acid addition and temperature. At the bottom of the table, ambient pH values are indicated for the initial solution mixture and the range of values observed at intervals during the ~96 h exposures

		Corrosion rate calculated from weight loss, mil/y		
in 280 g dU/L		temperature = 93-94˚C		
		excess sulfuric acid concentration		
specimen	location	0.01 M	0.10 M	0.25 M
Zr-4	immersed	0.03	0.02	0.00
Zr-4	vapor	0.00	0.02	0.00
ZrNb	immersed	0.00	0.00	0.00
ZrNb	vapor	0.00	0.00	0.00
316L	immersed	0.03	0.03	0.00
316L	vapor	0.02	0.00	0.00
2304	immersed	0.00	0.03	0.00
2304	vapor			
initial pH observed		0.56	0.49	0.38
pH range		0.52 - 0.67	0.37 - 0.49	0.27 - 0.39

For the convenience of the reader, Fig. 11 plots the average pH values (linear average of values for each of several different solutions prepared with the stated composition) for the different uranyl sulfate concentrations corresponding to 70, 140, and 280 g dU/L and the various excess sulfuric acid concentrations. The total range of pH observed over these experiments is about 0.4 to 1.0.

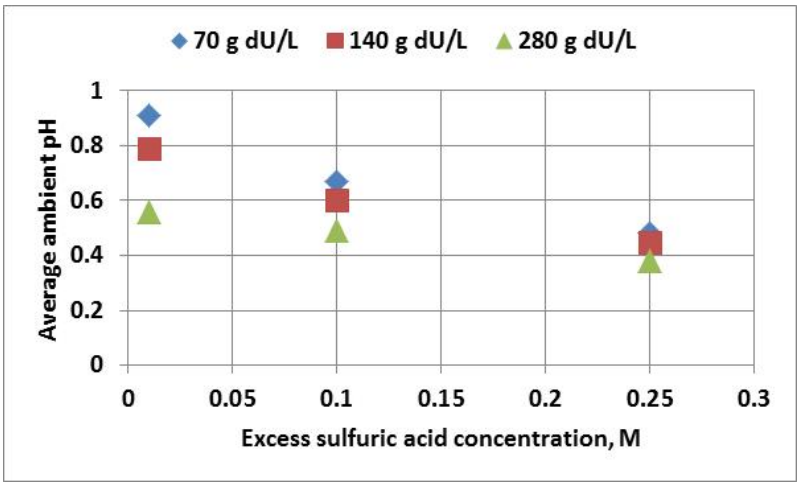

Fig. 11. Average ambient pH values as a function of uranyl sulfate and excess acid concentration for the static exposure results in Tables 7–9.

Table 10 shows the corrosion rate data determined for solutions similar to those previously described except for the addition of a modest quantity (0.25 M) of nitric acid to simulate increased oxidation potential as a result of radiolysis. Full immersion as well as exposure to vapor was accomplished for the primary candidate alloys in two different depleted uranyl sulfate concentrations, and this series of testing was performed at 80°C.

Table 10. Corrosion rates calculated from weight change for specimens exposed in uranyl sulfate corresponding to concentrations of 140 and 280 g dU/L with 0.25 M added nitric acid as a function of excess sulfuric acid addition at 80°C. At the bottom of the table, ambient pH values are indicated for the initial solution mixture and the range of values observed at intervals during the ~96 h exposures

all exposures 80-81˚C		Corrosion rate calculated from weight loss, mil/y					
0.25 M excess nitric acid							
		in 140 g dU/L			in 280 g dU/L		
		excess sulfuric acid concentration			excess sulfuric acid concentration		
specimen	location	0.01 M	0.10 M	0.25 M	0.01 M	0.10 M	0.25 M
Zr-4	immersed	0.00	0.00	0.00	0.04	0.00	0.00
Zr-4	vapor	0.00	0.04	0.00	0.00	0.01	0.00
ZrNb	immersed	0.00	0.00	0.00	0.00	0.00	0.00
ZrNb	vapor	0.00	0.01	0.00	0.00	0.01	0.00
316L	immersed	0.00	0.01	0.00	0.00	0.02	0.00
316L	vapor	0.00	0.02	0.00	0.00	0.00	0.00
2304	immersed	0.00	0.03	0.01	0.04	0.00	0.07
2304	vapor	0.00	0.00	0.00	0.02	0.00	0.03
initial pH observed		0.50	0.36	0.32	0.21	0.08	0.05
pH range		0.43 - 0.71	0.31 - 0.46	0.22 - 0.45	0.13 - 0.25	0.03 - 0.38	0.00 - 0.34

Similar to the previously described tests, the results for these conditions yielded only specimen weight changes so close to zero as to be near the discriminating capability of the scale; no calculated corrosion rates were larger than 0.07 mil/year. Also similar to the previous results, the zirconium-based alloys developed a very adherent light brown oxide sufficiently thin that the original machining marks on the specimen remained visible. The stainless steel specimens were not visibly changed as a result of exposure in the solutions containing nitric acid. Note that, compared with the previous tests, the pH of the solutions was about 0.2–0.5 pH units lower than for the equivalent solutions without nitric acid.

In addition, corrosion of all of the candidate alloys was evaluated at 93–94°C in a series of solutions with a 1 M excess of sulfuric acid and variable amounts of excess nitric acid (0.0, 0.25, and 1 M). The results are summarized in Table 11. Consistent with previous results, there was no significant difference in corrosion rate for a particular alloy as a function of uranium concentration or excess sulfuric acid concentration. As previously observed, the zirconium-based alloys developed a thin, adherent, light brown layer of ZrO_2, the primary stainless steel alloys (316L and 2304) revealed no readily visible changes associated with color and luster, and the surface roughness of all of the alloys was unchanged as a result of exposure. Figure 12 is representative of these observations. The equivalent specimens exposed in the vapor phase appeared very similar to immersed coupons shown in Fig. 12 except that, on the zirconium-based alloys, the light brown coloration was extremely faint and perhaps barely apparent.

Table 11. Corrosion rates calculated from weight change for specimens exposed in uranyl sulfate corresponding to a concentration of 140 g dU/L with 1 M added sulfuric acid as a function of excess nitric acid addition at 93–94°C. At the bottom of the table, ambient pH values are indicated for the initial solution mixture and the range of values observed at intervals during the ~96 h exposures

in 140 g dU/L and 1 M excess sulfuric acid		Corrosion rate calculated from weight loss, mil/y		
		temperature = 93-94°C		
		nitric acid concentration		
specimen	location	0 M	0.25 M	1.0 M
Zr-4	immersed	0.06	0.02	0.00
Zr-4	vapor	0.00	0.00	0.00
ZrNb	immersed	0.00	0.00	0.00
ZrNb	vapor	0.00	0.00	0.00
316L	immersed	0.03	0.04	0.00
316L	vapor	0.01	0.00	0.03
2304	immersed	0.00	0.00	0.07
2304	vapor	0.00	0.01	0.03
304L	immersed	0.60	0.17	0.24
304L	vapor	0.09	0.17	0.16
17-4 PH	immersed	0.59	0.84	0.96
17-4 PH	vapor	0.18	0.05	0.38
initial pH observed		0.13	0.06	-0.05
pH range		-0.01 to 0.17	-0.04 to 0.22	all < -0.05

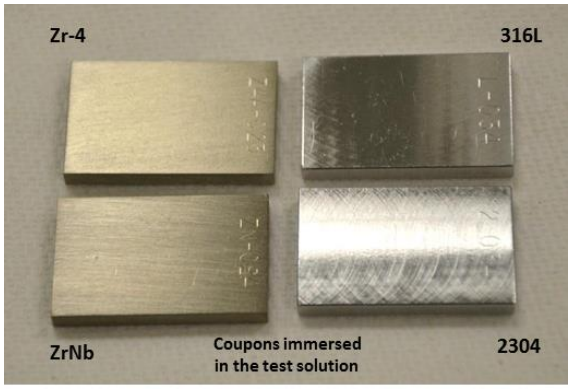

Fig. 12. Surfaces of primary candidate specimens following exposure at 94°C in uranyl sulfate at a concentration corresponding to 140 g dU/L with 1 M excess sulfuric acid and 0.25 M excess nitric acid additions for about 96 h. The brown coloration of the Zr-4 specimens is subtle; the contrast in the photo has been manipulated to enhance the difference between the zirconium alloys and stainless steels.

In contrast, the 304L and 17-4 PH alloys, both of which exhibited somewhat higher corrosion rates than the other stainless alloys in these environments, were substantially more affected in terms of discoloration and luster changes on the specimen surface. The examples in Figure 13 indicate that the 17-4 PH material was discolored to dark brown following immersion in the 140 g dU/L + 1 M sulfuric acid + 0.25 M nitric acid solution. However, the equivalent vapor phase coupon revealed only dark blue/black spots of localized discoloration. Neither type of discoloration could be wiped from the coupon surface, and the differently colored films perhaps relate to the different oxidation potentials for coupons fully immersed compared with those exposed in the vapor. Neither 304L specimen was dramatically changed; but the specimen exposed in the vapor phase exhibited some loss of luster as well as isolated spots of dark brown discoloration, whereas the immersed coupon was largely unchanged by the exposure.

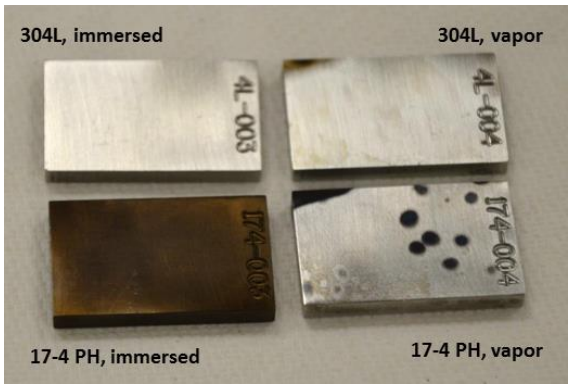

Fig. 13. Surfaces of 304L and 17-4 PH specimens following exposure at 94°C in depleted uranyl sulfate at a concentration corresponding to 140 g dU/L with 1 M excess sulfuric acid and 0.25 M excess nitric acid additions for about 96 h. The brown coloration of the Zr-4 specimens is subtle; the contrast in the photo was manipulated to enhance the difference between the zirconium alloys and stainless steels.

Additions of iodide species were also incorporated into the testing scheme. Initially, a series of exposures comparable to those already described was performed, with the inclusion of 25 wppm I^- (as KI) and 25 wppm IO_3^- (as KIO_3) added to a depleted uranyl sulfate concentration corresponding to 70 or 140 g dU/L with excess sulfuric acid additions (0.01, 0.10, and 0.25 M) at 94°C. It was recognized that a total of 50 wppm of iodide species was grossly in excess of any iodide concentration expected in the SHINE process, but the lack of corrosion observed in the initial exposures suggested significant acceleration of corrosion might be necessary to identify potential corrosion concerns.

Table 12 summarizes the corrosion rate data for the initial exposures to incorporate iodine species (50 wppm) into the solution. Of particular note is that, even at the relatively high exposure temperature of 94°C and an iodine concentration much higher than expected, the zirconium alloys remain quite resistant to general corrosion. As in the solutions without iodine, the zirconium alloys developed a very uniform and adherent light brown oxide, no surface roughness changes, and very limited weight losses corresponding to uniform corrosion rates of 0.1 mil/year or less. Also note that the solution pH values did not change appreciably as a function of the iodine additions.

Table 12. Corrosion rates calculated from weight change for specimens exposed in uranyl sulfate corresponding to a concentration of 70 or 140 g dU/L with 50 wppm iodine species added as a function of excess sulfuric acid addition at 93–94°C. At the bottom of the table, ambient pH values are indicated for the initial solution mixture and the range of values observed at intervals during the ~96 h exposures

50 wppm iodine species		Corrosion rate calculated from weight loss, mil/y					
test temperature 94°C							
		140 g dU/L			70 g dU/L		
		excess sulfuric acid concentration			excess sulfuric acid concentration		
specimen	location	0.01 M	0.10 M	0.25 M	0.01 M	0.10 M	0.25 M
Zr-4	immersed	0.10	0.03	0.00	0.03	0.01	0.00
Zr-4	vapor	0.00	0.03	0.00	0.00	0.01	0.00
ZrNb	immersed	0.00	0.04	0.00	0.00	0.00	0.03
ZrNb	vapor	0.00	0.06	0.00	0.00	0.00	0.00
316L	immersed	1.14	0.18	0.15	0.89	0.13	0.11
316L	vapor	4.35	0.98	1.11	5.88	0.81	0.48
2304	immersed	1.20	0.22	0.17	0.97	0.15	0.15
2304	vapor	2.07	1.38	0.18			
304L	immersed	0.45	0.07	0.07			
304L	vapor	2.20	0.31	0.20			
17-4 PH	immersed	0.22	0.26	0.46			
17-4 PH	vapor	2.98	0.56	0.18			
initial pH observed		0.84	0.65	0.50	1.05	0.82	0.61
pH range		0.69 - 0.86	0.52 - 0.69	0.33 - 0.53	0.99 - 1.05	0.75 - 0.82	0.51 - 0.61

In contrast, the stainless steels examined generally exhibited higher corrosion rates than were observed in the equivalent solutions without iodine additions. The stainless alloys seem particularly prone to corrosion in the vapor space above the solutions containing iodine additions. Specifically, for 13 of the 15 exposure pairs for which corrosion rates under vapor and immersion conditions can be compared, the coupon exposed in vapor yielded an average corrosion rate at least twice that of the immersed specimen. The greatest difference was near a factor of 13. None of the immersed stainless steel specimens was discolored significantly, and there was no apparent change in the surface roughness of the specimens. However, specimens exposed in the vapor phase often exhibited isolated dark red/brown corrosion product accumulation—not unlike the discoloration pattern observed on the vapor-phase 17-4 PH coupon shown in Fig. 13 – that adhered relatively poorly to the surface. The inability to completely remove the

corrosion product potentially introduced error in the corrosion rate calculation , tending to make the estimate too low if all the corrosion product were not removed. More important is the observation that, based on corrosion product distribution, the corrosion process itself was not uniform, which also may lead to underestimation of the local corrosion rate. Nevertheless, the highest general corrosion rate observed was less than 6 mil/year. It is not clear why the vapor-phase environment resulted in higher observed corrosion rates than immersion in most of these exposures; but it seems likely that the iodine species are somewhat volatile and escape the solution (as vapor/gas) and condense on surfaces above the solution line as salts or acids. This behavior has been observed by the author in association with hot nitric acid solutions with halide additions (chlorides and fluorides), but that is a much more oxidizing environment than the sulfate solutions under consideration in this work. In addition, the vapor phase may be somewhat more oxidizing simply because of the presence of additional air/oxygen at this location (potential in-leakage at the interface between beaker and condenser).

The data also suggest the trend of decreasing corrosion rate (in vapor and immersion) with increasing excess sulfuric acid concentration. Although it is not possible to dismiss that trend entirely, note that these tests were performed as a series in which the original solution (with 0.01 M excess acid and 50 wppm iodine species addition) was changed only by adding sulfuric acid in sequence to the original solution. Thus if in fact the iodine species are somewhat volatile and are not replenished, their concentration in these tests would be decreasing somewhat during the series of exposures. Because of concerns of this type about potential variability in the corrosivity of the test solution, particularly associated with the vapor phase, planned-interval testing was incorporated into the assessment.

A total of three planned-interval tests were performed in this reporting period. The first two such exposures used reduced iodine concentrations (compared with the initial level of 50 wppm) of 28 and 5 wppm. In both cases, the baseline solution had a uranyl sulfate concentration equivalent to 140 g dU/L and 0.10 M excess sulfuric acid concentration; and the iodine species were split approximately as half I^- from KI and half IO_3^- from KIO_3. The temperature in both exposures was maintained at 93–94°C, and the pH range observed for both solutions was 0.60–0.78. After examination of these results, a third planned-interval test was performed using the same baseline solution (140 g dU/L with 0.10 M excess sulfuric acid) incorporating 28 wppm iodine species. In the latter case, 0.25 M nitric acid was also added as a radiolysis simulant.

Table 13 summarizes the data gathered in the first two planned-interval tests comparing iodine concentrations. Several trends are apparent. Compared with the corrosion rates observed in the equivalent environment with 50 wppm iodine species added, the corrosion rates observed for *vapor*-phase exposure were lower for 28 wppm iodine and lower still for 5 wppm iodine. These results suggest stainless steel corrosion is a relatively strong function of iodine content within the liquid generating the vapor. The trend for the immersed specimens was less apparent, but overall the corrosion rates were much lower under immersion conditions and were largely independent of the iodine concentration. For the convenience of the reader, corrosion rate values for the stainless steels are presented as a function of iodine additions in Table 14; the rates observed in the A_4 exposures were used to compare the planned-interval test data with the single-exposure data of Table 12 (selecting the 0.10 M excess acid solution). It is evident that the corrosion rates for immersed specimens were much less sensitive to iodine concentration; with the possible exception of the 17-4 PH material, all of the immersed specimens exhibited low corrosion rates.

Table 13. Planned-interval test results for stainless steels exposed (immersion and vapor) to test solutions with 140 g dU/L and 0.10 M excess sulfuric acid as a function of iodine species additions at 93–94°C

28 wppm iodine		Corrosion rate, mil/y				5 wppm iodine		Corrosion rate, mil/y			
		304L	316L	2304	17-4 PH			304L	316L	2304	17-4 PH
immersion	A_1	1.00	0.07	0.08	0.40	immersion	A_1	0.19	0.23	0.00	0.38
	A_3	0.39	0.03	0.03	0.39		A_3	0.10	0.06	0.09	0.40
	A_4	0.27	0.03	0.01	0.31		A_4	0.09	0.05	0.05	0.41
	B_1	1.19	0.05	1.16 *	1.06		B_1	0.18	0.08	0.34	0.44
	A_{calc}	0.00	0.00	0.00	0.09		A_{calc}	0.07	0.04	0.00	0.45
vapor	A_1	0.06	0.06	0.50		vapor	A_1	0.09	0.06	0.25	
	A_3	0.28	0.02	0.76			A_3	0.02	0.00	0.09	
	A_4	0.24	0.66	0.39			A_4	0.03	0.03	0.07	
	B_1	0.30	0.31	0.28			B_1	0.02	0.18	0.26	
	A_{calc}	0.12	2.58	0.00			A_{calc}	0.06	0.08	0.00	
metal corrodibility											
	immersion	↓	↓	↓	↓			↓	↓	↓	≈
	vapor	↓	↑	↓				≈	↓	↓	
environment corrosivity											
	in liquid	≈	≈	≈	↑			≈	↓	↑	≈
	in vapor	↑	↑	↓				↓	↑	≈	
KEY:	↑ = factor is increasing				≈ = factor remains unchanged			↓ = factor is decreasing			

* = error suspected in recording of initial specimen weight; actual number suspected to be ~ 0.08

Table 14. Stainless steel corrosion rates as a function of iodine concentration for solutions of 140 g dU/L and 0.10 M excess sulfuric acid at 93–94°C

iodine species additions				
		Corrosion rate, mil/y		
		50 wppm	28 wppm	5 wppm
316L	immersed	0.18	0.03	0.05
	vapor	0.98	0.66	0.03
2304	immersed	0.22	0.01	0.05
	vapor	1.38	0.39	0.07
304L	immersed	0.07	0.27	0.09
	vapor	0.31	0.24	0.03
17-4 PH	immersed	0.26	0.31	0.41
	vapor	0.56		

The immersed stainless steel specimens in the planned-interval tests, in 28 wppm and 5 wppm iodine, were found to be generally shiny and pristine following exposure. The only exception was the 17-4 PH specimens immersed in these solutions. They tended to develop a pale blue/gray discoloration, but there was no evidence of a change in surface roughness. Specimens of each alloy exposed in the vapor phase

tended to develop a dull luster and spots of minor discoloration (generally toward reddish brown) that were most consistently present on the edges of the specimens. Rarely, modest corrosion product could be removed from these locations with aggressive wiping; but no change in surface roughness was detected in any case, despite an appearance similar to pitting in some cases. Figure 14 is representative of these observations.

At the bottom of Table 13, the key analysis points for the first two planned-interval tests are summarized. Perhaps the most significant finding is that the corrodibility of the immersed metal specimens decreased as a function of time for seven of the eight alloy/environment combinations listed (for the other, the corrodibility remained unchanged). This suggests that the passive film that formed during the initial corrosion activity upon exposure to the environment was quite stable and protective. Similarly, metal corrodibility generally decreased for specimens exposed in the vapor phase, although the 316L specimen in 28 wppm iodine solution was observed to become somewhat more corrodible.

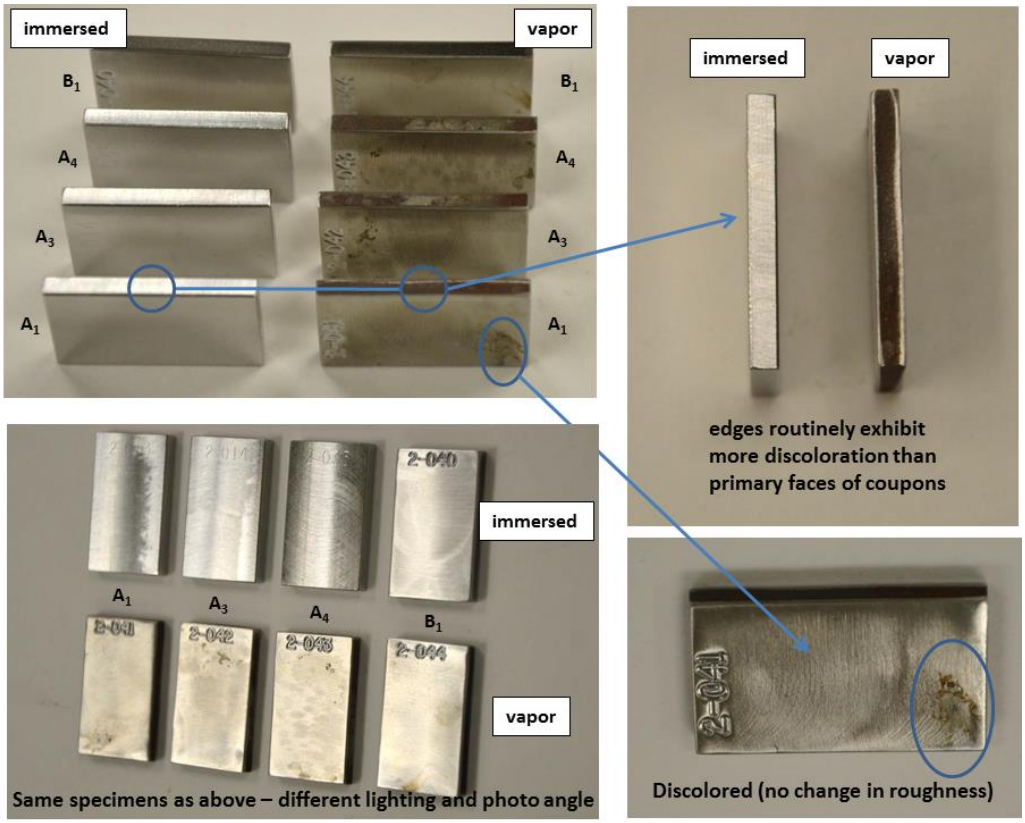

Fig. 14. Type 2304 stainless steel coupons following planned-interval testing for eight total days in a solution containing 140 g dU/L with 0.10 M sulfuric acid and 28 wppm iodine species at 94°C.

The corrosivity of the environment was found to increase in the vapor phase for three of the six alloy/environment combinations listed in Table 13. This finding is consistent with the speculation regarding the relative volatility of the halide species in these solutions (which may have been much more prominent in the exposures with 50 wppm iodine species added, but these were not examined under the planned-interval protocol). The change in the corrosivity of the liquid was more diverse—six of eight alloy/environment combinations yielded no change or a decrease in corrodibility, while two combinations revealed a clear increase. In a practical sense, the changes in the environment are not as significant to material selection provided that the metal tends to form a stable passive film as indicated in these exposures.

An additional planned-interval test was performed to compare corrosion patterns for two solutions with 28 wppm iodine species added, one with and one without 0.25 M nitric acid added as a radiolysis simulant. All other factors (baseline solution composition and test temperature) remained the same, although the pH of the solution with nitric acid was 0.49–0.55, about 0.1–0.2 pH units more acidic than the equivalent solution with no nitric acid. Table 15 summarizes the results, which reveal little in the way of a consistent pattern among the corrosion rates observed. Comparing A_1 and A_4 values, three of four immersed alloys (304L is the exception) showed higher corrosion rates with the nitric acid added to the solution; but even the highest rate among these, 1 mil/year, has little engineering significance. Corrosion rates for coupons exposed to vapor reveal even less regular trends among the very low values. However, it seems that 316L tended to exhibit higher vapor corrosion rates in the presence of nitric acid; whereas, at least for several exposure durations, the other two alloys in vapor exhibited slightly lower rates with nitric acid. Among the stainless steels examined, it might be expected that 316L would be the one most negatively affected by the presence of nitric acid: the combination of relatively low chromium content and high nickel and Mo content compared with the other alloys renders 316L relatively more susceptible to the oxidizing power provided by nitric acid. However, based on the low corrosion rates observed in all cases, any such effect was modest for these exposure conditions.

Table 15. Planned-interval test results for stainless steels exposed (immersion and vapor) to test solutions of 140 g dU/L and 0.10 M excess sulfuric acid with 28 wppm iodine species, with and without 0.25 M nitric acid addition, at 93–94°C

0.25 M nitric acid added										
28 wppm iodine		Corrosion rate, mil/y				28 wppm iodine		Corrosion rate, mil/y			
		304L	316L	2304	17-4 PH			304L	316L	2304	17-4 PH
immersion	A_1	0.24	0.23	0.13	0.54	immersion	A_1	1.00	0.07	0.08	0.40
	A_3	0.14	0.11	0.04	0.38		A_3	0.39	0.03	0.03	0.39
	A_4	0.11	0.10	0.10	0.76		A_4	0.27	0.03	0.01	0.31
	B_1	0.33	0.17	0.16	0.51		B_1	1.19	0.05	1.16 *	1.06
	A_{calc}	0.04	0.07	0.30	1.92		A_{calc}	0.00	0.00	0.00	0.09
vapor	A_1	0.14	0.18	0.11		vapor	A_1	0.06	0.06	0.50	
	A_3	0.06	0.17	0.04			A_3	0.28	0.02	0.76	
	A_4	0.06	0.77	0.06			A_4	0.24	0.66	0.39	
	B_1	0.14	0.56	0.45			B_1	0.30	0.31	0.28	
	A_{calc}	0.08	2.55	0.13			A_{calc}	0.12	2.58	0.00	
metal corrodibility						metal corrodibility					
	immersion	↓	↓	↑	↑		immersion	↓	↓	↓	↓
	vapor	↓	↑	↓			vapor	↓	↑	↓	
environment corrosivity						environment corrosivity					
	in liquid	≈	≈	≈	≈		in liquid	≈	≈	≈	↑
	in vapor	≈	↑	↑			in vapor	↑	↑	↓	
KEY:	↑ = factor is increasing				≈ = factor remains unchanged			↓ = factor is decreasing			
				* = error suspected in recording of initial specimen weight; actual number suspected to be ~ 0.08							

Examination of the metal corrodibility trends suggests that the addition of nitric acid negatively influenced alloys 2304 and 17-4 PH when they were immersed but had no substantial effect on metal corrodibility in the vapor. There was little overall effect on the corrosivity of the immersion environment; but the vapor became more corrosive with nitric acid, based on the response of 2304 specimens. In terms of appearance, the specimens immersed in the nitric acid–bearing solution generally appeared shiny and

pristine as they did after immersion in the other solutions. An exception was the 17-4 PH material, which tended to turn a blue/gray color that darkened with exposure time (see Fig. 15). The specimens exposed in vapor were also similar to others in this series; a general loss of luster and isolated spots of red/brown discoloration (mostly on coupon edges) was routinely observed.

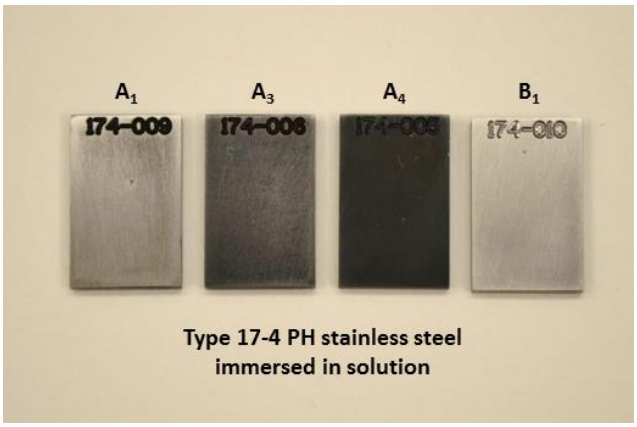

Fig. 15. Type 17-4 PH stainless steel planned-interval test coupons following exposure immersed in 140 g dU/L with 0.10 M excess sulfuric acid, 28 wppm iodine species, and 0.25 M nitric acid at 93–94°C.

In sum, the planned-interval exposures indicated that corrosion of the stainless steels is somewhat sensitive to an iodine concentration in the range of 5–50 wppm, particularly as it relates to metallic surfaces in the vapor phase. However, the trend toward reduced corrosion (immersion and vapor phase) with decreasing iodine concentration suggests that, at the levels expected in the SHINE process (on the order of 0.1–1.0 ppm), it is unlikely that iodine species will generate a general corrosion problem for the candidate stainless steels. Future tests will consider the possibility of stress-corrosion cracking of candidate alloys in the presence of iodine species in solution.

A total of 96 galvanic exposures were performed in this study, with each test incorporating one of the zirconium alloys coupled directly with one of the stainless steels under investigation. Table 16 summarizes the entire set of galvanic couples and environmental conditions for exposure.

The pattern of results among all galvanic couple exposures suggested no changes in corrosion behavior compared with behavior observed for the individually exposed specimens (with no galvanic coupling). For example, all of the zirconium alloys developed and maintained a light golden brown coloration consistent with the film appearance noted for individual specimens exposed. Similarly, no changes in surface roughness or indications of pitting or accelerated corrosion were observed at/near locations of direct contact with stainless steel, and calculated corrosion rates were all less than 0.1 mil/year. Types 316L and 2304 stainless steel did not develop discoloration or increased surface roughness in any of the exposures, and corrosion rates were uniformly less than 0.1 mil/year. The performance of type 17-4 PH stainless steel specimens coupled to zirconium alloys also was essentially indistinguishable from that of the uncoupled specimens. Each was uniformly tarnished to some degree with a blue/gray color of an intensity/darkness depending particularly on the presence of nitric acid, iodine, and temperature. The type 17-4 PH coupled specimens had calculated corrosion rates consistent with those observed for uncoupled specimens (generally in the range of 0.2 to 1.5 mil/year, although rates near 3 mils/y were observed in high iodine concentrations, consistent with standard immersions). Figure 16 shows representative specimens following galvanic corrosion testing.

Table 16. Summary of galvanic couple exposure test combinations

uranyl sulfate corresponding to g dU/L	excess sulfuric acid, M	temperature ˚C	excess nitric acid, M	iodine additions wppm	couples
140	0.01	80-81			Zr-4 with each of 316L, 2304, 17-4 PH
140	0.10	80-81			Zr-4 with each of 316L, 2304, 17-4 PH
140	0.25	80-81			Zr-4 with each of 316L, 2304, 17-4 PH
140	0.01	80-81	0.25		Zr-4 with each of 316L, 2304, 17-4 PH
140	0.10	80-81	0.25		Zr-4 with each of 316L, 2304, 17-4 PH
140	0.25	80-81	0.25		Zr-4 with each of 316L, 2304, 17-4 PH
140	1.00	80-81	0.00		ZrNb with each of 316L, 2304, 17-4 PH
140	1.00	80-81	0.25		ZrNb with each of 316L, 2304, 17-4 PH
140	1.00	80-81	1.00		ZrNb with each of 316L, 2304, 17-4 PH
140	0.10	80-81		9	ZrNb with each of 316L, 2304, 17-4 PH
140	0.10	80-81		14	ZrNb with each of 316L, 2304, 17-4 PH
140	0.10	80-81		30	ZrNb with each of 316L, 2304, 17-4 PH
140	0.01	93-94			Zr-4 with each of 316L, 2304, 17-4 PH
140	0.10	93-94			Zr-4 with each of 316L, 2304, 17-4 PH
140	0.25	93-94			Zr-4 with each of 316L, 2304, 17-4 PH
140	0.01	93-94	0.25		Zr-4 with each of 316L, 2304, 17-4 PH
140	0.10	93-94	0.25		Zr-4 with each of 316L, 2304, 17-4 PH
140	0.25	93-94	0.25		Zr-4 with each of 316L, 2304, 17-4 PH
140	0.10	93-94		28	ZrNb with each of 316L, 2304, 17-4 PH
140	0.10	93-94		50	ZrNb with each of 316L, 2304, 17-4 PH
70	0.10	93-94		0	Zr-4 and ZrNb with each of 316L, 2304, 17-4 PH
70	0.10	93-94		7	Zr-4 and ZrNb with each of 316L, 2304, 17-4 PH
70	0.10	93-94		28	Zr-4 and ZrNb with each of 316L, 2304, 17-4 PH
280	0.10	93-94		0	Zr-4 and ZrNb with each of 316L, 2304, 17-4 PH
280	0.10	93-94		7	Zr-4 and ZrNb with each of 316L, 2304, 17-4 PH
280	0.10	93-94		28	Zr-4 and ZrNb with each of 316L, 2304, 17-4 PH

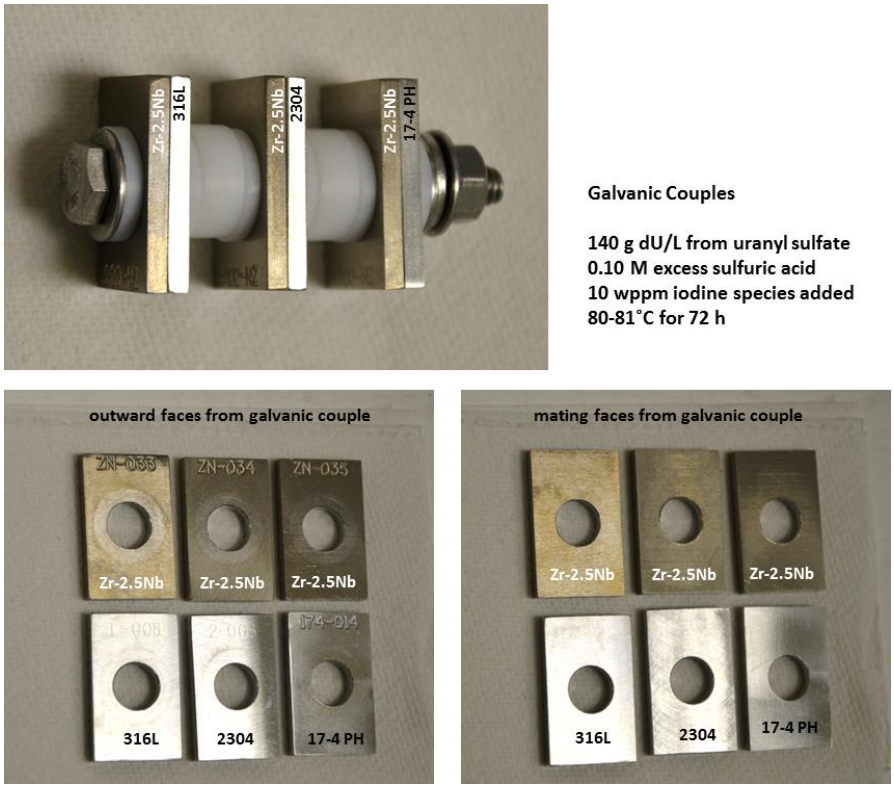

Fig. 16. Representative appearance of specimens following galvanic exposure in the given conditions. Note in particular that the mating faces appear identical to the "non-contact" faces of each couple. Lighting and contrast for this photo tend to exaggerate the relative brown coloration of the zirconium alloys.

Because of the limited duration of the galvanic tests (~72 h) and the relatively significant variability in corrosion rates for a marginally passive material like 17-4 PH, it cannot be stated for certain that absolutely no acceleration in corrosion for 17-4 PH resulted from coupling with zirconium alloys. However, no change in coloration or surface roughening—that is, no gradient relative to contact with the zirconium alloys—was observed on any 17-4 PH specimen. Should interest in 17-4 PH become more intense as the design stage progresses, longer-duration testing should be considered for specific couples of interest.

Limited cavitation testing at room temperature was performed on zirconium alloys (Zr-4 and ZrNb) and stainless steels (316L, 2304, and 17-4 PH) in the baseline solution (140 g dU/L, 0.10 M excess sulfuric acid) and in a similar solution (described in Sect. 3) in which the uranyl sulfate was replaced with sodium sulfate. The purpose of the comparison was to identify any potential for significant differences in erosion/corrosion resistance of the alloys in an environment in which the passive film on the alloys was routinely disturbed by high-velocity fluid (in this case, simulated by the sonication treatment). Figure 17 displays representative data for specimen weight loss as a function of sonication time. The weight change per unit of exposure time is often highly variable in the early stages of such a test, primarily because variations in surface hardness (as a general material property and a result of the influence of specimen preparations such as polishing/grinding) influence the incubation time for developing sufficient damage to generate a measureable weight change.

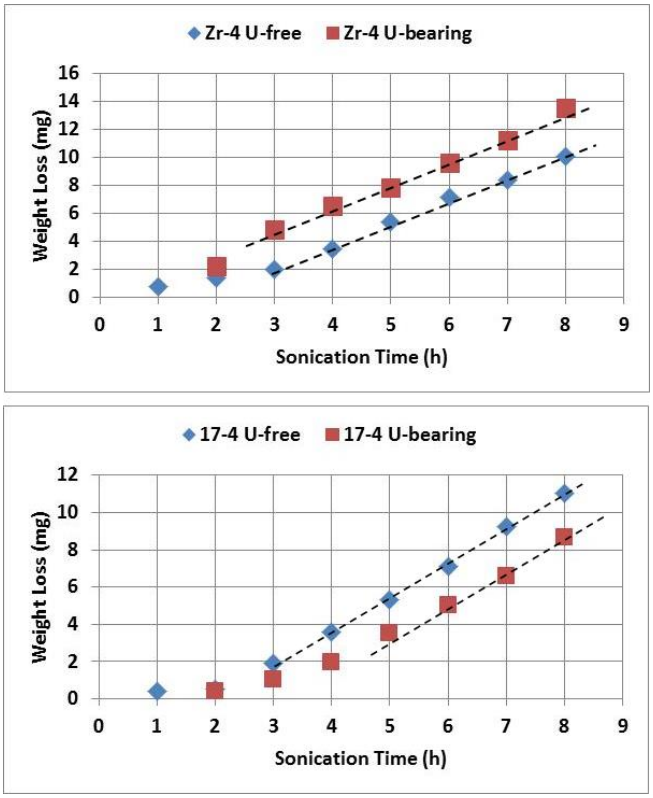

Fig. 17. Weight loss as a function of sonication time for Zr-4 (top) and 17-4 PH (bottom). Dotted lines on each plot represent approximate slopes for the weight change as a function of sonication time (each hour on the graph is 30 minutes sonication and 30 minutes of static corrosion). The data compare results for sonication in uranium-bearing solutions and roughly equivalent solutions free of uranium species.

The most important detail of Fig. 17 for the present study is that the rate of weight change per unit of time at extended exposures, when a steady-state interaction develops, is essentially independent of the solution composition for each alloy. That is, Zr-4 is degraded similarly in the uranyl sulfate and the sodium sulfate solutions, suggesting that uranyl sulfate introduces no erosion/corrosion component in the process environment that is missing from a similar uranium-free solution. Visually, the zirconium specimens sonicated in each solution appear to be identical: they show only uniform roughening of the surface (no pits or craters) and no golden brown film formation as a result of the low-temperature environment and the constant removal of films via sonication. Similarly, 17-4 PH responded with erosion/corrosion rates that were indistinguishable in solutions with and without uranyl sulfate. In the example data shown here, 17-4 PH stainless steel (diamond pyramid hardness 322) resisted the initiation of steady-state weight loss longer than did Zr-4 (DPH = 190) primarily because 17-4 PH was significantly harder. The hardness might also encourage lower long-term weight loss, but it apparently has little/no effect on the individual alloy response to the solution composition. Curiously, the total weight loss observed was higher in the uranium-free solution for four of the five materials studied, with only Zr-4 having a slightly higher weight loss in the uranium-bearing solution. However, all materials, independent of the solution, exhibited a weight loss rate in the range of 1.6–1.8 mg/h at steady state.

Ultimately, the preliminary conclusion from the cavitation exposures to date is that flow velocity in the SHINE process is unlikely to have an effect that is not also present for simple water systems free of uranium. The design basis can proceed accordingly. Plans for future work call for incorporation of additional cavitation experiments, as well as rotating disc experiments in an electrochemical cell to examine potential velocity effects.

5. CONCLUSIONS

A substantial collection of technical literature associated with the execution of the HRT and related experiments HRE-1 and HRE-2 in the 1950s at ORNL was reviewed. It documented relevant experience related to the compatibility of candidate zirconium alloys and stainless steels in the environment(s) of the proposed SHINE process to produce ^{99}Mo. This information clearly indicated that zirconium-based alloys and stainless steels similar in composition to type 347 performed extremely well (very low corrosion rates; no failures) in HRT laboratory experiments and operations at temperatures, flow rates, and power levels considerably more aggressive than those expected in the SHINE process.

To confirm those trends under more SHINE-relevant conditions, several candidate alloys— Zr-4, Zr-2.5Nb, 316L, 2304, 304L, and 17-4 PH—were tested under exposure to potentially corrosive environmental conditions. The alloys were subjected to static exposure in solutions representing a wide range of temperatures, uranyl sulfate concentrations, excess sulfuric acid concentrations, nitric acid additions (to simulate radiolysis product generation), and iodine additions.

In all cases, corrosion of the zirconium alloys was observed to be minimal: corrosion rates based on weight loss were calculated at <0.1 mil/year with no changes in surface roughness. In all cases, the corrosion film was identified with XPS to be ZrO_2 of varying thickness that influenced coloration (toward light brown for thicker films). Galvanic coupling with various stainless steels in selected exposures had no discernable effect on appearance, surface roughness, or corrosion rate. Based on these results, a preliminary corrosion allowance of 0.1 mil/year for zirconium-based alloys seems reasonable as a process design parameter; additional information is expected to result from gamma irradiation exposures planned in FY 2015.

Corrosion of the stainless steels was also modest across the entire range of exposures. With limited exceptions associated with iodine additions to the test solutions, all stainless steels were highly resistant to SHINE process simulants. They demonstrated corrosion rates of <1 mil/year, no discoloration, and no changes in surface roughness. In a few of the most aggressive variants of prototypic solutions, type 17-4 PH was observed to develop a dark brown or black interference film; but low corrosion rates and no changes in surface roughness remained a consistent result. None of the stainless steels was observed to exhibit accelerated corrosion as a result of galvanic coupling with zirconium-based alloys in selected exposures.

The stainless steels under investigation revealed some sensitivity to iodine concentration in the prototypic test environments, particularly for exposure within the vapor phase. Note that the testing incorporated higher temperatures than are expected in the SHINE process and dramatically higher iodine concentrations than expected (by a multiple of 50–500); both factors were intended to accelerate potential corrosion reactions without changing the primary corrosion mechanism. With that caveat, at the highest concentrations of iodine (50 wppm) examined, maximum general corrosion rates of about 1.2 mil/year were observed for immersed stainless steels, which remained shiny and exhibited no change in roughness or luster. Somewhat higher corrosion rates (~6 mil/year) were observed for specimens exposed to vapor—particularly early in the exposure period—and isolated spots of discoloration suggested the possibility of localized corrosion. However, lower concentrations of iodine species (5 and 28 wppm) were much less corrosive; and the planned-interval data indicated metal corrodibility decreased with time for all immersed exposures and, with one minor exception, all vapor exposures. Little change in susceptibility to corrosion was observed as a result of adding nitric acid to the test environment (simulating radiolysis products). The trend toward reduced corrosion (immersion and vapor phase) with decreasing iodine concentration suggests that, at the expected conditions in the SHINE process (on the

order of 0.1–1.0 wppm, temperatures ≤ 80°C), it is unlikely that iodine species will generate a general corrosion concern for the candidate stainless steels.

Consistent with the literature data reviewed, type 304L and 17-4 PH stainless steels were observed to be somewhat more susceptible to corrosion as a function of excess sulfuric acid (up to 1 M) than their 2304 and 316L counterparts. This result was expected because of the higher total alloy content (primarily Cr and Mo, respectively) of the latter materials. Although all corrosion rates observed were quite modest in 1 M excess sulfuric acid, the results suggest that preference should be given to types 316L and 2304 as offering more corrosion resistance in the general environment (uranyl sulfate and sulfuric acid) and more room for error with regard to corrosion than the other stainless steels. To the extent possible, it might be preferable to specify them in selecting alloys for piping and other related components (e.g., pumps, seals, instruments).

Because of the wider range of results associated with the stainless steels than with the zirconium-alloys, determination of a corrosion allowance applicable to all exposure scenarios for the stainless steels remains uncertain. Based on corrosion test results in this research, a working allowance of 1 mil/year for preliminary design considerations seems generally conservative for each of the candidate alloys, pending more information relative to the potential for corrosion associated with iodine species in solution.

Erosion/corrosion behavior was independent of the test solution, uranyl sulfate or sodium sulfate solution adjusted to a similar pH, suggesting no negative effect of uranium results from fluid dynamic conditions aggressive to the passive film. Cavitation conditions are not expected in the SHINE process, but this technique was used to explore the response of candidate alloys under conditions particularly aggressive to the passive film.

Based on these results and to account for process conditions that cannot be fully anticipated, such as changing environments resulting from radiolysis, it is recommended that the process design incorporate witness coupons as a method to monitor process corrosion. Particularly early in the process, gathering corrosion data from specimens representing the actual containment alloys in service would provide an opportunity to anticipate maintenance requirements or identify shortcomings in the design.

Future tests (FY 2015 and beyond) will use electrochemical testing of stainless steels in iodine-bearing solutions to further examine passivity characteristics. Additional planned-interval immersions (and vapor exposures) will likely be incorporated to support the electrochemical testing. The stress-corrosion cracking behavior of candidate alloys will also be examined via U-bends or other techniques, with particular emphasis on performance in the presence of iodine species in solution. In addition, fluid velocity factors will continue to be explored via additional vibratory horn testing as well as rotating disc electrode techniques.

6. REFERENCES

1. G. R. Piefer, K. M. Pitas, E. N. Van Abel, T. R. Mackie, T. A. Heltemes, R. V. Bynum, T. T. Gribb, and R. F. Radel, "Mo-99 Production Using a Subcritical Assembly, " in *Proceedings of the First Annual Molybdenum-99 Topical Meeting*, December 4–7, 2011, Santa Fe, NM.

2. "Morgridge Institute for Research, with partner SHINE Medical Technologies, receives new round of federal funding for $85M medical isotope project," press release for Morgridge Institute for Research and SHINE Medical Technologies, May 8, 2012.

3. J. A. Lane, H. G. McPherson, and Frank Maslan, eds., *Fluid Fuel Reactors*, Addison-Wesley, 1958. (A particularly relevant subset of the information is incorporated as Part I: Aqueous Homogenous

Reactors, J. A. Lane, ed.; and Chapter 5, Integrity of Metals in Homogenous Reactor Media, by E. G. Bohlmann, et al. addresses potential corrosion in some detail.)

4. E. G. Bohlmann and G. M. Adamson, *Stress Corrosion Cracking Problems in the Homogenous Reactor Test*, Central Files letter report CF-57-1-143, Oak Ridge National Laboratory, January 31, 1957.

5. H. C. Savage, G. H. Jenks, and E. G. Bohlmann, *In-Pile Test Loops for Aqueous Homogenous Reactor Solutions*, Technical Report ORNL-2977, Oak Ridge National Laboratory, December 21, 1960.

6. *ASM Handbook of Corrosion Data*, ASM International, Metals Park, OH, 1989; extracted from J. E. Truman, *Corrosion: Metal-Environment Reactions*, Vol. 1, L. L. Shreir, ed., Newness-Butterworths, p. 352, 1976.

7. *ASM Handbook of Corrosion Data*, ASM International, Metals Park, OH, 1989; extracted from *A Guide to Corrosion Resistance*, Climax Molybdenum Company, Greenwich, CT, 1981.

8. Electronic mail correspondence from E. Van Abel (SHINE Medical Technologies) to S. Pawel (Oak Ridge National Laboratory), "Iodine in Target Solution," April 30, 2014.

9. *Standard Practice for Laboratory Immersion Corrosion Testing of Metals*, Standard ASTM G31, American Society for Testing and Materials, West Conshohocken, PA, 1990.

10. *Standard Method of Vibratory Cavitation Erosion Test*, Standard ASTM G32, American Society for Testing and Materials, West Conshohocken, PA, 2009.